Chemical Geology xxx (2017) xxx–xxx

Contents lists available at ScienceDirect

Chemical Geology

journal homepage: www.elsevier.com/locate/chemgeo

Tracking the onset of Phanerozoic-style redox-sensitive trace metal enrichments: New results from basal Ediacaran post-glacial strata in NW Canada

Austin J. Miller [a], Justin V. Strauss [b], Galen P. Halverson [c], Francis A. Macdonald [d], David T. Johnston [d], Erik A. Sperling [a,*]

[a] Department of Geological Sciences, Stanford University, Stanford, CA 94305, USA
[b] Department of Earth Sciences, Dartmouth College, Hanover, NH 03755, USA
[c] Department of Earth and Planetary Sciences, McGill University, Montreal, Quebec, H3A 2A7, Canada
[d] Department of Earth and Planetary Sciences, Harvard University, Cambridge, MA 02138, USA

ARTICLE INFO

Article history:
Received 7 November 2016
Received in revised form 2 March 2017
Accepted 5 March 2017
Available online xxxx

Keywords:
Ediacaran
Sheepbed Formation
Windermere Supergroup
Oxygen
Redox-sensitive trace metals
Molybdenum
Uranium

ABSTRACT

A global rise in oxygen levels has been proposed to coincide with the Ediacaran to Cambrian radiation of animals, yet the precise timing and nature of this change remains unresolved. One hypothesis is that the ocean/atmosphere system became temporarily well-oxygenated in the earliest Ediacaran, directly following the Marinoan Snowball Earth glaciation (~635 Ma). The evidence for oxygenation is based on large enrichments of redox-sensitive trace elements in black shale from South China presumably deposited under a euxinic water column. These enrichments meet or exceed the bulk concentrations of redox-sensitive trace elements found in Phanerozoic shale deposited under euxinic water columns. Here we test the early Ediacaran post-Snowball oxygenation hypothesis with new data from a high-resolution, multi-proxy geochemical and sedimentological study of three stratigraphic sections in the earliest Ediacaran Sheepbed Formation of the Mackenzie and Wernecke Mountains, NW Canada. Iron speciation data from all sections suggest that the local water column was dominantly ferruginous, with a notable exception of probable euxinic conditions recorded in part of one section. Redox-sensitive elements show no appreciable enrichments in the basal Sheepbed Formation, with maximum concentrations of molybdenum, vanadium, uranium and chromium only slightly above world average shale values. The lack of substantial elemental enrichments within the Sheepbed Formation is consistent with results from coeval ferruginous strata in Svalbard. The dominance of local ferruginous conditions in NW Canada cannot alone account for the muted redox-sensitive element enrichments as V, U, and Cr are thought to be enriched under these conditions, and samples deposited under euxinic conditions also lack Phanerozoic-style enrichments. These contrasting results from different localities highlight a need to further investigate the veracity of trace metal enrichments in all localities as representing global redox conditions as the results have important implications for the timing of oxygenation with respect to early animal evolution.

1. Introduction

The Ediacaran Period (ca. 635 Ma–541 Ma) witnessed a variety of profound environmental changes, including the termination of low-latitude Snowball Earth glaciations, large perturbations to the geochemical cycles of carbon and sulfur, and dynamic redox shifts in the Earth's ocean/atmosphere system (Fike et al., 2006; Halverson et al., 2010; Lyons et al., 2014). During this pivotal time in Earth's history, there was a radical shift in the fossil record from mostly microscopic prokaryotic assemblages to large, complex macrofossils in the mid- to late-Ediacaran and finally to the shelly animal fauna of the Cambrian (Xiao and Laflamme, 2009; Erwin et al., 2011). Although the relationship is not established with certainty, a rise in oxygen is commonly believed to have played a fundamental role in biological evolution through the Ediacaran-Cambrian transition, acting either directly in factors such as body size, or indirectly in allowing for the evolution of predators and a resulting predator-prey 'arms race' (Sperling et al., 2013a).

Geochemical redox proxies from global sedimentary successions have been used to reconstruct an array of temporal hypotheses for the timing of ocean/atmosphere oxygenation during the terminal Neoproterozoic. Initial studies, focused on iron speciation and sulfur isotopes ($\delta^{34}S$), proposed widespread oxygenation following the ca. 580 Ma Gaskiers glaciation (Canfield et al., 2007; Fike et al., 2006). In

* Corresponding author.
E-mail address: esper@stanford.edu (E.A. Sperling).

http://dx.doi.org/10.1016/j.chemgeo.2017.03.010
0009-2541/

contrast, more recent work focused on redox-sensitive element (RSE) enrichments from South China has promoted a more nuanced oxygenation history, where oxygen levels rose substantially in the earliest Ediacaran following the ca. 635 Ma Marinoan glaciation (Sahoo et al., 2012). This evidence lends support to the hypothesis that a post-glacial nutrient surplus fueled ocean oxygenation (Elie et al., 2007; Kirschvink et al., 2000; Kunzmann et al., 2013, 2015; Planavsky et al., 2010). The evidence for high oxygen levels (based on RSE enrichments; discussed below) abruptly disappears in the early Ediacaran (Sahoo et al., 2012), leading to the suggestion that this transitory first spike in oxygen levels was one of several transitory Ocean Oxygenation Events (OOEs) punctuating a generally reducing Ediacaran ocean (Sahoo et al., 2016).

Redox-sensitive elements have great utility in addressing the global areal extent of oxic conditions at the sediment-water interface. Many of these elements have relatively low crustal abundances and low riverine fluxes from oxidative weathering in surface environments (Emerson and Huested, 1991; Turekian and Wedepohl, 1961). These attributes, combined with their long residence times in seawater, allow them to be used to track the global ocean redox state (Emerson and Huested, 1991). For elements such as uranium, molybdenum, vanadium and chromium, deposition in sediment under reducing water columns is their most effective sink (Emerson and Huested, 1991; Tribovillard et al., 2006). Therefore, the major control on the RSE concentrations in seawater is the geographic extent of these reducing sinks, specifically the global proportion of reducing versus oxic conditions at the sediment-water interface (Algeo, 2004; Emerson and Huested, 1991; Gill et al., 2011; Morford and Emerson, 1999; Owens et al., 2016; Partin et al., 2013b; Pearce et al., 2008; Reinhard et al., 2013; Sahoo et al., 2012; Sahoo et al., 2016; Scott et al., 2008). If the area of reducing environments is expanded beyond a critical threshold, the sinks outpace the source flux, resulting in a net decrease of RSE concentrations in seawater (Fig. 1; Sahoo et al., 2012; Scott et al., 2008). Because authigenic sediment enrichment is positively correlated to seawater RSE concentrations (e.g., Algeo and Lyons, 2006; Scott et al., 2013a), sediment deposited under anoxic water columns during times of globally expansive reducing conditions will display comparatively low RSE enrichments. The opposite is also true—as oceans become well-oxygenated, seawater RSE concentrations should increase globally, resulting in a distinct fingerprint of high RSE enrichments in local anoxic sedimentary basins, akin to those recorded in Phanerozoic anoxic shale (i.e., 'Phanerozoic-style' enrichments; Fig. 1; Sahoo et al., 2012; Scott et al., 2008). Thus, RSE enrichments in strata known to be deposited under anoxic conditions can be informative about the global redox landscape.

In South China, an early Ediacaran pulse of RSE enrichments in Mo (to 172 mg/kg), V (to 6417 mg/kg), and U (to 33 mg/kg) was observed in black shale of Member II of the Doushantuo Formation, directly above Marinoan glacial deposits and the associated cap carbonate, and interpreted to represent ephemeral global ocean oxygenation (Sahoo et al., 2012). Multiple RSE concentration spikes up-section in the Doushantuo Formation at the Wuhe locality were used as evidence to suggest this post-Marinoan event was the first of several OOEs (Sahoo et al., 2016). Depleted pyrite sulfur isotope ratios from these same stratigraphic intervals were interpreted as the result of an expanded seawater sulfate reservoir, consistent with global oxygenation (Sahoo et al., 2012, 2016). These OOEs have been labeled sequentially through time, with the first post-Marinoan enrichment termed OOE-A. If the global ocean was well oxygenated during these OOEs, other localities worldwide should either: 1) exhibit an oxic signature, or 2) be interpreted as anoxic and record similar patterns of 'Phanerozoic-style' enrichments in RSEs. Neither appears to be the case for data published to date from other coeval localities. For example, iron speciation data from Svalbard highlights a persistently ferruginous to sub-oxic shelf environment throughout the Neoproterozoic with muted Mo, V, and U concentrations (Kunzmann et al., 2015). Iron speciation data from the Wernecke Mountains of Yukon also show a dominantly ferruginous shelf environment at the beginning of the Ediacaran with muted Mo and V enrichments (Johnston et al., 2013). However, direct comparison of the RSE records in these studies with the basal Ediacaran record of South China is challenging due to differences in sampling density, poor temporal constraints on sampled sections, predominance of ferruginous conditions preserved in other Ediacaran successions (rather than euxinic conditions as in modern analogues), and the extremely condensed nature of the South China sections compared to normal marine shale successions.

The Ediacaran stratigraphic record in NW Canada provides an excellent location to test the transitory OOE framework proposed by Sahoo et al. (2012, 2016). Here, we present new multi-proxy geochemical data

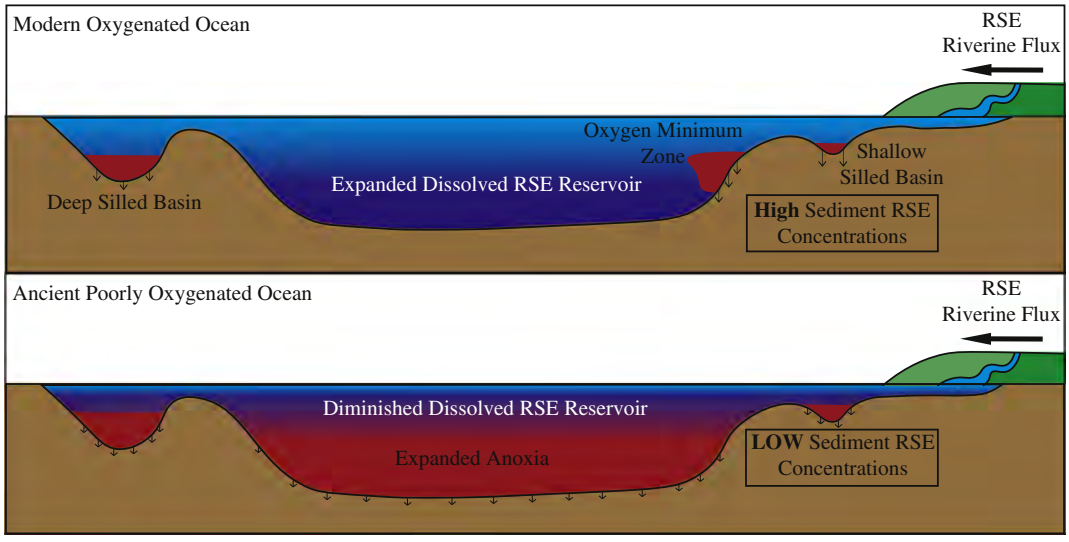

Fig. 1. A comparison of modern oxygenated and ancient poorly oxygenated ocean RSE cycling. The main RSE sinks are sediments deposited under reducing conditions. As anoxic conditions are rare in the modern ocean, the oceanic RSE inventory is high. Because authigenic RSE enrichment is a function of dissolved RSE levels, anoxic shale deposited in the modern (and much of the Phanerozoic) exhibit large RSE enrichments. Conversely, in ancient poorly oxygenated oceans, the areal extent of anoxic conditions can crash the dissolved RSE reservoirs in seawater. As a result, sediment deposited underneath an anoxic water column would exhibit muted enrichments. See Algeo (2004), Scott et al. (2008), Sahoo et al. (2012), and text for further discussion.

Please cite this article as: Miller, A.J., et al., Tracking the onset of Phanerozoic-style redox-sensitive trace metal enrichments: New results from basal Ediacaran post-glacial str..., Chem. Geol. (2017), http://dx.doi.org/10.1016/j.chemgeo.2017.03.010

from three basal Ediacaran sections of the Sheepbed Formation along a shelf-to-basin transition. Ultimately these data help to elucidate global marine redox conditions in the wake of one of the largest climatic perturbations in Earth's history, the Marinoan glaciation, and help to further resolve the temporal history of Neoproterozoic oxygenation and its possible relationship (if any) to the evolving eukaryotic biota.

2. Background

2.1. Iron speciation

Using RSE enrichments to infer the global redox landscape requires independent evidence that the host strata were deposited under anoxic conditions. We reconstructed local redox conditions using the iron speciation proxy on fine-grained strata, which distinguishes between oxic, ferruginous, and euxinic depositional environments (Poulton and Canfield, 2011; Raiswell and Canfield, 1998). This redox proxy divides iron found in shale into two pools based on biogeochemical reactivity. The highly reactive (Fe_{HR}) pool comprises pyrite (Fe_{Py}) and species that are reactive with sulfide on early diagenetic timescales, including iron carbonates, iron (oxyhydr)oxides and magnetite. The remainder of total iron (Fe_T) resides in the poorly reactive and unreactive pool, made up predominantly of iron in phyllosilicate minerals. In the modern ocean, samples deposited under an oxic water column have a $Fe_{HR}/Fe_T < 0.38$, while samples deposited under an anoxic water column generally have $Fe_{HR}/Fe_T > 0.38$ (Raiswell and Canfield, 1998). Anoxic environments can be characterized by the presence of either excess free sulfide (i.e., euxinic) or ferrous iron (i.e., ferruginous). Where $Fe_{HR}/Fe_T > 0.38$, ratios of $Fe_{Py}/Fe_{HR} > 0.7–0.8$ indicate pyrite as the main constituent of the highly reactive iron pool, implying euxinic depositional conditions, whereas $Fe_{Py}/Fe_{HR} < 0.7–0.8$ indicates deposition in a ferruginous environment with unsulfidized reactive iron (Anderson and Raiswell, 2004; März et al., 2008; Poulton and Canfield, 2011).

2.2. Redox-sensitive trace elements

RSEs concentrations within shale are governed by a balance of detrital and authigenic fluxes to the sediment, the latter being useful to reconstruct marine redox conditions. RSEs are generally soluble under oxic conditions, but they become insoluble and/or complex with organic matter, sulfides, or other metals under reducing conditions, resulting in authigenic enrichments (Tribovillard et al., 2006). RSEs are conventionally normalized to biogeochemically conservative elements such as Al or Ti to account for variability in detrital flux (e.g., Calvert and Pedersen, 1993), as well as to total organic carbon (TOC) due to its influence on authigenic enrichments within the sediment. As the sequestration pathways (particularly with respect to sulfide presence) are important for interpreting RSEs as a global tracer, these mechanisms are reviewed below for Mo, V, U and Cr.

Molybdenum is conservative and present in high concentrations (~105 nM) in modern oxic seawater where it is present as the molybdate anion (MoO_4^{2-}) (Morford et al., 2005). In oxic environments, Mo deposition is controlled by the slow adsorption onto Fe and Mn-oxyhydroxides (Bertine and Turekian, 1973). In anoxic environments, when $[H_2S_{(aq)}]$ is >~11 μM there is a quantitative switch from MoO_4^{2-} to tetrathiomolybdate (MoO_xS_{4-x}), which increases particle reactivity and facilitates subsequent removal from the water column into the sediment (Erickson and Helz, 2000; Helz et al., 1996). The exact pathways of sequestration within the sediment column remains an area of active research, but observations of positive correlation between Mo and TOC suggest organic matter is associated with the dominant removal mechanism in euxinic settings (Algeo and Maynard, 2004; Chappaz et al., 2014). In the modern ocean, Mo requires euxinic conditions in the upper pore water or water column in order to develop significant authigenic enrichments (Dahl et al., 2013; Little et al., 2015; Scott and Lyons, 2012), which limits its utility as a paleo-redox proxy in pervasively ferruginous Neoproterozoic oceans (Canfield et al., 2008; Guilbaud et al., 2015; Sperling et al., 2015).

Vanadium is quasi-conservative and exists in seawater at high concentrations (~35–45 nM) primarily as the vanadate ionic species (HVO_4^{2-} and $H_2VO_4^-$) in modern oxic oceans (Huang et al., 2015). In these environments, V is tightly coupled to the redox cycling of Fe- and Mn-oxyhydroxides. In mildly reducing conditions, vanadium reduction should occur in the low-Eh zone of denitrification prior to sulfate reduction (Piper and Isaacs, 1996). In such environments, V(V) is reduced to the V(IV) species that can be removed from the water column by adsorption processes and the formation of organo-metallic ligands. In the presence of $H_2S_{(aq)}$ in experimental studies, V(IV) is further reduced to V(III) that can be taken up by geoporphyrins or precipitate in a solid oxide phase (V_2O_3 or $V(OH)_3$) (Wanty and Goldhaber, 1992). Thus, although V is expected to be enriched under anoxic but non-euxinic conditions, the stepwise reduction involving the presence of sulfide may allow for varying levels of enrichment between ferruginous and euxinic environments (Algeo and Maynard, 2004; Scott et al., 2017). In contrast to these experimental and ancient sedimentary geochemical studies, in some modern natural highly euxinic settings V may remain in the water column due to organic ligand complexation or other confounding biogeochemical factors (e.g., Algeo and Maynard, 2008; Emerson and Huested, 1991). Consequently more information is needed to truly understand the role of sulfide in vanadium cycling.

Uranium is conservative in oxic environments, and is present as uranyl ions that often complex with carbonate ions to form $UO_2(CO_3)_3^{4-}$, with a mean concentration in modern seawater of ~14 nM (Ku et al., 1977). Uranium is predominantly buried in sediments below low-oxygen to anoxic water columns (Anderson et al., 1989; Klinkhammer and Palmer, 1991). Modern studies suggest that uranium reduction does not readily occur in the water column (Anderson et al., 1989; Van der Weijden et al., 1990), but rather within reducing sediments through abiotic and biotic pathways (Bargar et al., 2013; Behrends and Van Cappellen, 2005; Hsi and Langmuir, 1985; Lovley and Phillips, 1992; Zheng et al., 2002). Precipitation within the sediment occurs through the formation of organo-metallic ligands with humic acid, absorption onto ferric iron hydroxides, or the direct formation of uraninite or metastable precursors (Hsi and Langmuir, 1985; Klinkhammer and Palmer, 1991; Zheng et al., 2002). Laboratory experiments have recently shown that hydrogen sulfide and ferrous iron both exhibit rapid rates of reduction kinetics resulting in the quantitative reduction of U(VI) to U(IV) (Massey et al., 2014; Stylo et al., 2015). Together these factors suggest U should be valuable in tracking global redox states under both euxinic and ferruginous conditions. However, use of U as a local and global redox proxy is complicated by strong controls from sedimentation rate and organic carbon burial. Thus, variation in uranium concentrations within ancient anoxic strata may not perfectly reflect changes in the overall redox landscape of the ocean (Calvert and Pedersen, 1993; Emerson and Huested, 1991; Klinkhammer and Palmer, 1991; McManus et al., 2005).

Chromium predominantly exists as the chromate anion (CrO_4^{2-}) in oxic water columns, with minor concentrations of the reduced aquahydroxyl ion $Cr(H_2O)_4(OH)_2^+$ (Calvert and Pedersen, 1993). Chromium reduction in mildly denitrifying conditions from Cr(IV) to Cr(III) forms $Cr(OH)_2^+$, $Cr(OH)_3$, or $(Cr, Fe)(OH)_3$, which can complex with humic or fulvic acids and absorb to Fe- and Mn-oxyhydroxides, generating authigenic enrichments (Algeo and Maynard, 2004; Tribovillard et al., 2006; Piper and Calvert, 2009). Euxinia is not necessary for Cr enrichment because it does not form an insoluble sulfide. Interpretations of chromium's authigenic enrichment in sediment are complicated by its relatively large detrital flux relative to the overall enrichment levels (Tribovillard et al., 2006).

Please cite this article as: Miller, A.J., et al., Tracking the onset of Phanerozoic-style redox-sensitive trace metal enrichments: New results from basal Ediacaran post-glacial str..., Chem. Geol. (2017), http://dx.doi.org/10.1016/j.chemgeo.2017.03.010

2.3. Geologic background

2.3.1. Regional stratigraphy and tectonostratigraphic framework

The ca. 780–540 Ma Windermere Supergroup (Young et al., 1979) of the Mackenzie and Wernecke Mountains, NW Canada, is an ~6 km-thick mixed siliciclastic-carbonate sedimentary succession that consists of, in stratigraphically ascending order, the Coates Lake, Rapitan, Hay Creek, and "upper" groups (Turner et al., 2011 and references therein, Fig. 2). In the Hay Creek Group, the upper Stelfox Member of the Ice Brook Formation has been correlated with Marinoan-age glacial deposits worldwide and is capped by the ca. 635 Ma Ravensthroat and Hayhook cap carbonate that define the base of the Ediacaran Period (James et al., 2001; Knoll et al., 2006; Narbonne and Aitken, 1995). The informal "upper" group begins with transgressive shale deposits of the Sheepbed Formation, which were recently dated with Re-Os geochronology to 632.3 ± 5.9 Ma (Rooney et al., 2015). The Sheepbed Formation is overlain by mixed siliciclastic and carbonate strata of the 'June beds' and Gametrail and Blueflower formations, which contain Ediacara-type fossil impressions (Macdonald et al., 2013; Narbonne and Aitken, 1990; Narbonne et al., 2014). An unconformity at the top of the Risky Formation, the stratigraphically highest unit in the "upper group," broadly marks the Ediacaran-Cambrian boundary (Narbonne and Aitken, 1995).

Traditionally, the Windermere Supergroup is thought to have been deposited along a thermally subsiding passive margin (e.g., Eisbacher, 1981; Narbonne and Aitken, 1995; Ross, 1991). For example, the Coates Lake and Rapitan groups have been characterized as rift-related deposits filling narrow extensional basins associated with the opening of the proto-Pacific Ocean (Ross, 1991), with a prominent transition to passive margin sedimentation coinciding with the basal Twitya Formation (Narbonne and Aitken, 1995; Ross, 1991). However, this tectonic model is complicated by the presence of synsedimentary faulting throughout the Hay Creek and "upper" groups in the Mackenzie Mountains (Aitken, 1991; Eisbacher, 1981, 1985; Jefferson and Parrish, 1989),

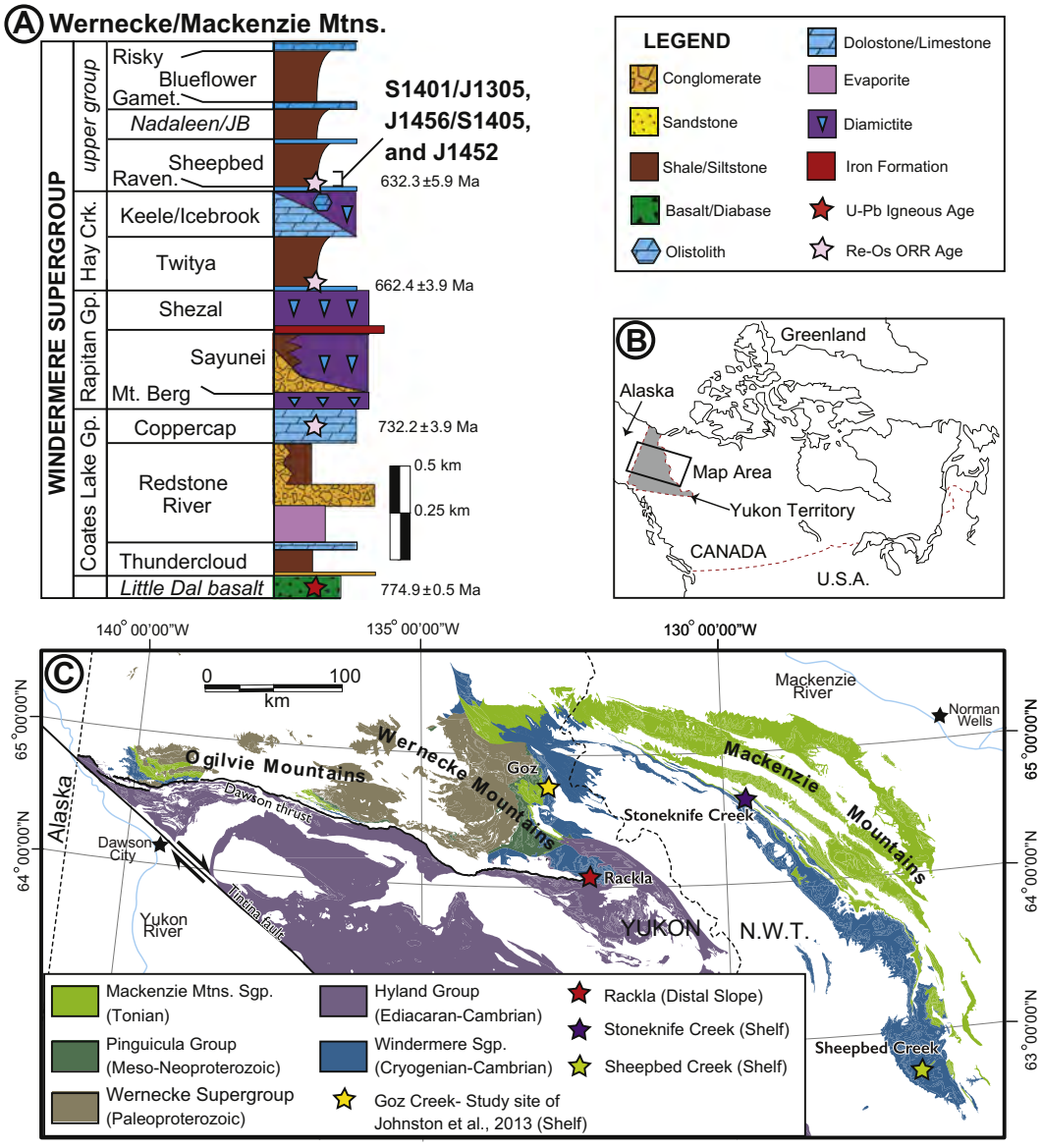

Fig. 2. (A) Generalized stratigraphy of the Windermere Supergroup, Wernecke and Mackenzie Mountains, Yukon and Northwest Territories. Illustrated stratigraphic height is schematic and varies across the region. Italics indicate informally named units. Column is modified from Strauss et al. (2015). U-Pb age on Little Dal Basalt is from Jefferson and Parrish (1989), U-Pb ages from base of Rapitan Group are from Macdonald et al. (2010), and Re-Os ages are from Rooney et al. (2014, 2015). Sections S1401/J1305, S1405/J1456, and J1452 span the basal Sheepbed Formation. Raven. - Ravensthroat, JB - June Beds, Gamet. - Gametrail. (B) Regional map of Canada illustrating the study area. (C) Neoproterozoic exposure across the northern Canadian Cordillera, after Strauss et al. (2015). Stars indicate localities of this study and Goz Creek, the study locality of Johnston et al. (2013). Environments of deposition are assigned based on regional context and stratigraphic interpretations at each locality.

Please cite this article as: Miller, A.J., et al., Tracking the onset of Phanerozoic-style redox-sensitive trace metal enrichments: New results from basal Ediacaran post-glacial str..., Chem. Geol. (2017), http://dx.doi.org/10.1016/j.chemgeo.2017.03.010

and evidence of extensional tectonism and diachronous volcanism throughout upper Neoproterozoic and lower Cambrian strata in the southern Canadian and U.S. Cordillera (Colpron et al., 2002; Lund et al., 2003, 2010; Yonkee et al., 2014). Thus, a more complicated history of the Cordilleran margin is emerging, with topographic development and distinct rifting events in the Cryogenian and Ediacaran (Macdonald et al., 2013; Strauss et al., 2015; Yonkee et al., 2014).

The regional depositional environment is important for utilizing RSEs to distinguish global redox signals (e.g., Algeo and Lyons, 2006; Algeo and Rowe, 2012). For example, the isolation of basinal water masses from the open ocean can generate localized drawdown of RSEs due to hydrographic restriction. In NW Canada, the geometry and degree of connection of the basin in which the Sheepbed Formation was deposited is imperfectly understood. Nonetheless, pervasive slope deposits (Dalrymple and Narbonne, 1996; Narbonne and Aitken, 1995; MacNaughton et al., 2000), possible contourites in the June beds at Sekwi Brook (Dalrymple and Narbonne, 1996), and the continuity of Ediacaran shelf and slope deposits across ~900 km of strike-length suggest a substantially open marine margin.

2.3.2. Locality stratigraphic descriptions

The geochemistry of the basal Sheepbed Formation was studied in detail at a shelf locality at Stoneknife Creek, Northwest Territories, and at a newly described distal slope locality in the Rackla belt, Yukon (Fig. 2). A more stratigraphically expanded study of the Sheepbed Formation was conducted near its type section at Sheepbed Creek, Northwest Territories (Gabrielse et al., 1973), providing the first geochemical data on this time interval from sections in the southern Mackenzie Mountains. With the exception of samples from the basal Sheepbed Formation in the Rackla belt, samples exhibiting alteration or possible secondary pyrite were avoided during sampling.

2.3.2.1. Stoneknife Creek - J1452 - stratigraphic description. At Stoneknife Creek, the Ravensthroat cap carbonate consists of 7.4 m of finely laminated, buff-yellow peloidal dolograinstone with 0.3–1.5 m-thick cuspate bedforms, overlain by 3.0 m of thin-bedded dolomudstone/dolosiltstone packages in 0.5 m-thick coarsening-upwards cycles (Fig. 3). These strata are overlain by a 17.2 m-thick fining-upwards package of interbedded lime mudstone and very fine-grained grainstone with calcareous black shale of the Hayhook Formation. A transition from predominantly carbonate to siliciclastic detritus occurs at ~28 m with the replacement of interbedded grainstone units with <0.5 cm thick quartz siltstone stringers, which we define as the base of the Sheepbed Formation. Laminae rich in pyrite were common in the transition into the Sheepbed and were avoided due to the possibility of post-depositional concentration (as in Sahoo et al., 2012).

2.3.2.2. Rackla - S1401/J1305 - stratigraphic description. Two parallel sections were measured ~100 m apart to document the diverse sedimentological characteristics of the Ravensthroat cap carbonate at this locality (see Supplemental information). This unit consists of a 2.6 m-thick, bright orange-yellow, very fine-grained dolograinstone with local sheet-crack cements (Fig. 4). A silty limestone unit (up to 3.9 m thick) is locally present above the cap dolostone in section J1305, but disappears along strike toward section S1401. This unit is considered here to be a local equivalent of the Hayhook Formation (James et al., 2001; Macdonald et al., 2013). The Hayhook strata are overlain by jet-black shale of the Sheepbed Formation. Shale samples directly above the cap carbonate are bleached and have an orange and yellow hematite and limonite weathering rind, suggesting that the samples were likely altered. Nonetheless, this interval was sampled to determine if this zone exhibited RSE enrichments. Black shale samples above 6.6 m did not show field evidence of alteration.

2.3.2.3. Sheepbed Creek - S1405/J1456 - stratigraphic description. Over 400 m of Sheepbed strata were measured and sampled at the Sheepbed Creek type section (Fig. 5; See also Supplemental information). Here, the Ravensthroat and Hayhook Formations are transitional with the basal Sheepbed Formation, and the lithostratigraphic boundary is placed at 9.7 m, where carbonate units become dispersed and discontinuous. By 14 m the Sheepbed here is >70% shale and contains minor siltstone and fine sandstone horizons. The frequency of siltstone and sandstone horizons within the Sheepbed Formation increases in the upper part of the section locally, with a transition to sandstone- and siltstone-dominated facies at ~350 m. This progression is consistent with observations from other measured sections of the Sheepbed Formation (Dalrymple and Narbonne, 1996; Gabrielse et al., 1973; Macdonald et al., 2013; MacNaughton et al., 2008; Sperling et al., 2016).

3. Materials and methods

126 shale samples were collected from measured sections (see Supplemental information for GPS coordinates and relationship of parallel sections). Samples were washed, cleaned, and cut to small chips using a water saw with a diamond blade. Samples were then crushed to flour in a tungsten carbide grinding container, which does not introduce substantial contamination for the elements of interest (Hickson and Juras, 1986, Sperling et al., 2013b). Major elements were determined using a Spectro Xepos X- ray fluorescence spectrometer with a helium gas flush in the EM-1 lab at Stanford University. To determine trace element concentrations, samples went through a two-step digestion using HCl-HF-HNO_3 followed by aqua regia at Geotop, Montréal, Québec, before being measured on a Thermo Finnigan iCAP Q inductively coupled plasma mass spectrometer (ICP-MS) at McGill University. Iron in carbonate, (oxyhydr)oxide, and mixed valence state (i.e., magnetite) iron pools were determined using sequential iron extraction following the methods outlined in Poulton and Canfield (2005). The amount of iron extracted was quantified using the ferrozine method described in Stookey (1970), which has similar reproducibility to flame AA or ICP-OES methods (Kunzmann et al., 2015). The amount of iron in the pyrite phase was determined through the chromium reducible sulfur method (CRS) of Canfield et al. (1986) and stoichiometric calculation from the captured sulfide. Fifteen samples chosen for their high Fe_{Py}/Fe_{HR} ratios were tested for the presence of Acid Volatile Sulfide (AVS) using the hot acid extraction method of Rice et al. (1993), with no measureable AVS removed from any sample tested. An aliquot of each sample was decarbonated in 1 M HCl then analyzed for TOC content and organic carbon isotope ratios via combustion in a Carlo Erba Elemental Analyzer and measurement of the resulting gas on a Finnegan MAT Delta Plus at Stanford University in continuous flow mode. Samples with low organic carbon content and/or high carbonate content were decarbonated using a 3 M solution of HCl, rinsed three times with DI water, loaded in tin capsules and combusted in a Carlo Erba Elemental Analyzer in the EM-1 lab at Stanford University. A subset of samples was run using both methods with good agreement between datasets (Table S1). The precision of each geochemical analysis can be found in the Supplemental information (Table S2–S5).

4. Results

Iron speciation results, TOC, and concentrations of RSEs of shale samples are plotted alongside their respective stratigraphic logs in Figs. 3–6. Organic carbon $\delta^{13}C$ values and RSE concentrations normalized to Al, Ti, and TOC are presented in the Supplemental information (Fig. S1–3). Raw data can be found in Supplemental information (Table S1).

4.1. Stoneknife Creek, Mackenzie Mountains – section J1452

Throughout the Stoneknife section, fine-grained samples are characterized by $Fe_{HR}/Fe_T > 0.38$, indicating a continuously anoxic water column (Fig. 3). A majority of samples exhibit $Fe_{Py}/Fe_{HR} < 0.70$, with highly reactive iron occurring mostly in carbonate or pyrite phases. A

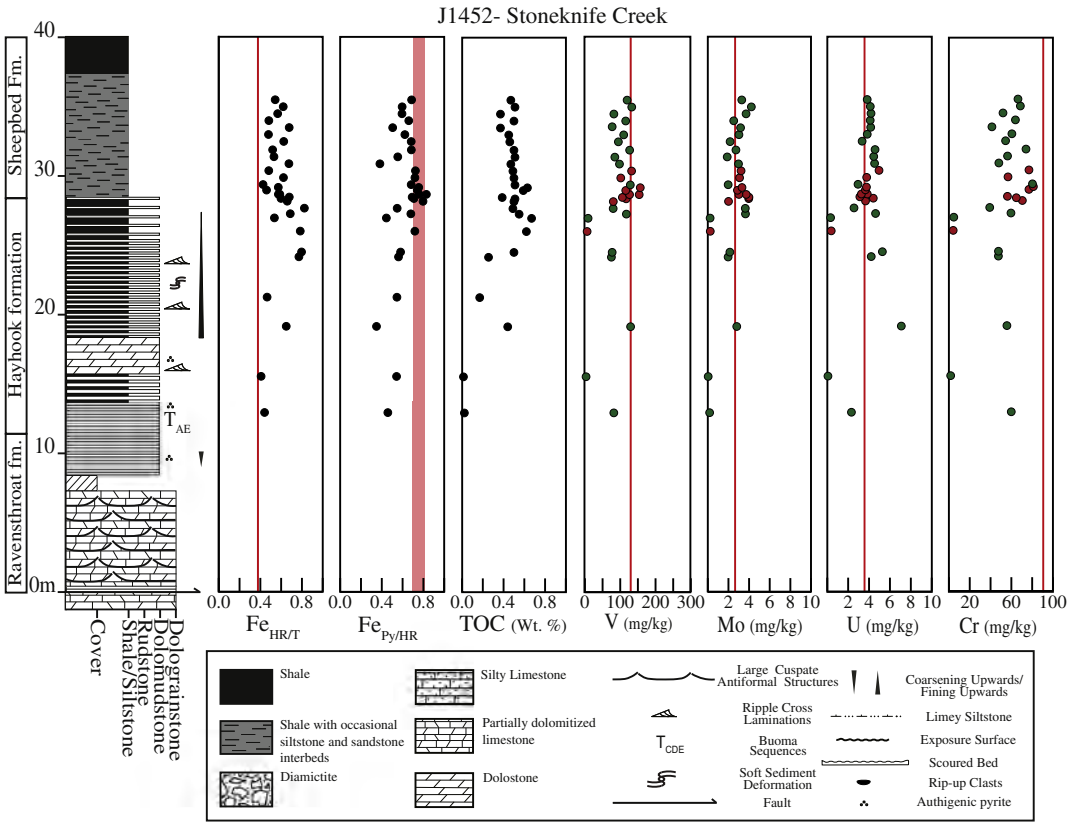

Fig. 3. Stratigraphic column of section J1452 at Stoneknife Creek, Northwest Territories. J1452 begins at the top of the Ice Brook Formation and continues through the Ravensthroat formation, Hayhook formation, and basal part of the Sheepbed Formation. From left to right data is plotted with relevant baseline values illustrated by vertical red lines; iron speciation highly reactive iron to total iron (Fe_{HR}/Fe_T; red line = 0.38), pyrite iron to highly reactive iron (Fe_{Py}/Fe_{HR}; red band = 0.7–0.8), weight percent total organic carbon, vanadium (red line = 130 mg/kg), molybdenum (red line = 2.6 mg/kg), uranium (red line = 3.7 mg/kg), and chromium (red line = 90 mg/kg). Redox-sensitive elements (RSEs) are plotted as concentrations in mg/kg and the vertical red lines indicate world average shale values (Turekian and Wedepohl, 1961). These RSE concentrations are similar to those of upper continental crust (McLennan, 2001). RSE data points are colored based off interpretations of iron speciation data, which should represent local water conditions at the time of deposition (green - ferruginous, red - euxinic, blue - oxic). (For interpretation of the references to color in this figure legend, the reader is referred to the web version of this article.)

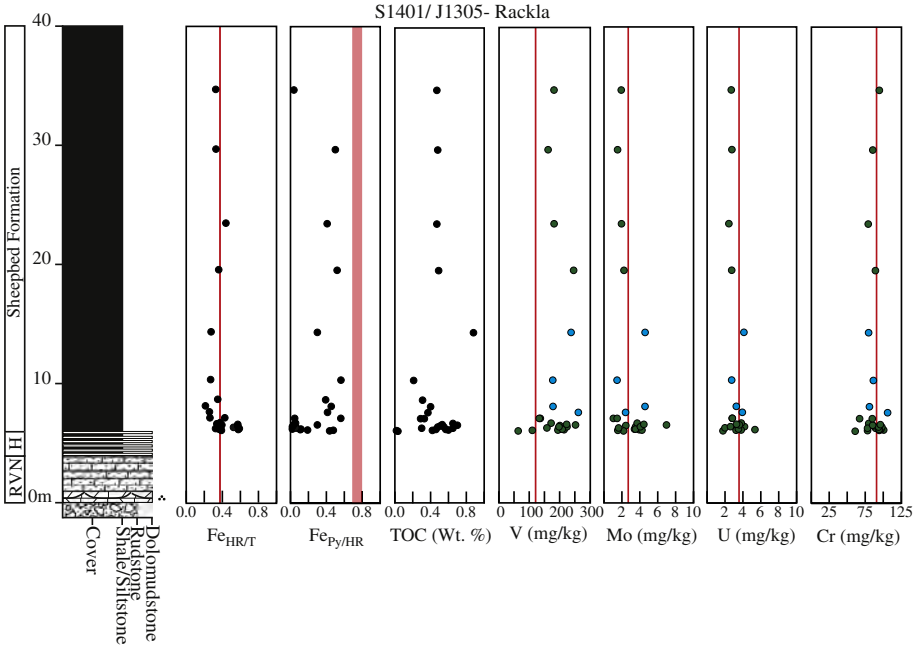

Fig. 4. Stratigraphic column of sections J1305 and S1401 in the Rackla belt, Wernecke Mountains, Yukon. These sections begin at the top of the Ice Brook Formation and measure through the Ravensthroat formation (RVN), Hayhook formation (H) and the basal part of the Sheepbed Formation. See Fig. 3 for information on geochemical plots and lithological symbols.

Please cite this article as: Miller, A.J., et al., Tracking the onset of Phanerozoic-style redox-sensitive trace metal enrichments: New results from basal Ediacaran post-glacial str..., Chem. Geol. (2017), http://dx.doi.org/10.1016/j.chemgeo.2017.03.010

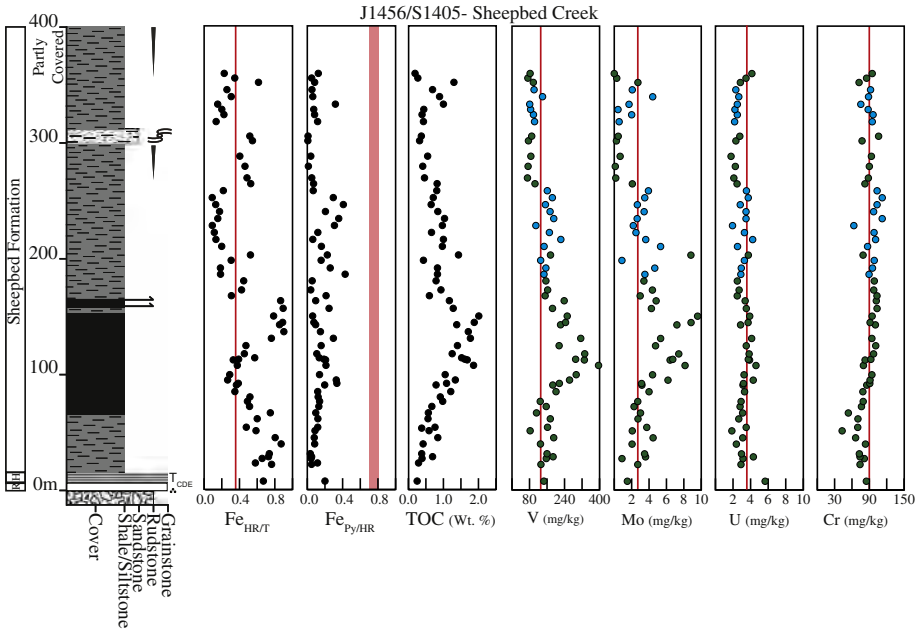

Fig. 5. Stratigraphic column of sections J1456 and S1405 at Sheepbed Creek, Mackenzie Mountains, Northwest Territories, near the type section of the Sheepbed Formation (Gabrielse et al., 1973). These sections begin at the top of the Ice Brook Formation and measure through the Ravensthroat formation (R), Hayhook formation (H), and the Sheepbed Formation until beds begin to coarsen upwards at ~400 m. Note change in scale with respect to Figs. 2 and 3; this section represents a longer-term record of the Sheepbed Formation rather than a detailed study of the immediate post-Marinoan interval. See Fig. 3 for information on geochemical plots and lithological symbols.

notable exception is in the upper Hayhook and basal Sheepbed strata, where samples consistently have $Fe_{Py}/Fe_{HR} > 0.70$. These changes likely represent a shift from deposition under a dominantly ferruginous environment to a period of stable euxinia before returning to ferruginous conditions in the upper part of the measured section. Vanadium, molybdenum, and uranium concentrations all exhibit similar patterns in relation to the world shale average (Turekian and Wedepohl, 1961), with consistent values at or just below average shale. Maximum enrichments of these elements occur in the euxinic interval but are muted, with maximum concentrations of 157, 4, and 7.1 mg/kg, respectively. Chromium exhibits a similar pattern of generally invariant concentration up-section, but all samples have lower concentrations than average shale, with a maximum of 81 mg/kg. TOC progressively increases stratigraphically upward throughout the measured section from 0.05 to 0.74 wt% at 28.6 m, coincident with the euxinic interval, before stabilizing around 0.5 wt% for the remainder for the section. RSEs remain at or below average shale values when normalized to Al and Ti (Fig. S1), and similarly RSEs normalized to TOC content do not show pronounced enrichments (Fig. S1). Titanium/Aluminum ratios, which can track mafic versus felsic provenance (Young and Nesbitt, 1998), are consistently low compared to average shale through the section, with an average value of 0.037 (Fig. S1). Organic carbon isotopes from the Stoneknife Creek section are invariant at ~ −31‰ (Fig. S1).

4.2. Rackla belt, Wernecke Mountains – sections J1305/S1401

Basal shale samples from the Sheepbed Formation at Rackla have heterogeneous Fe_{HR}/Fe_T ratios, with some samples exhibiting enrichments in Fe_{HR} ($Fe_{HR}/Fe_T > 0.38$) while others fall below this ratio (Fig. 4). Specifically, samples taken from 6.6 to 14.3 m have $Fe_{HR}/Fe_T < 0.38$, suggesting deposition under an oxic water column. For the rest of the section Fe_{HR}/Fe_T ratios are in the equivocal space of iron speciation (Poulton and Canfield, 2011; Sperling et al., 2016) just above or just below 0.38. All samples have Fe_{Py}/Fe_{HR} ratios falling well below 0.7. RSE enrichments are similar to average shale in V, Mo, U and Cr, and samples from 6.6 to 14.3 m do not show a distinct shift in RSE concentrations. Samples from the upper part of the section are slightly enriched in V (261 mg/kg), with no enrichments in Cr and minor depletions in Mo and U. TOC content varies from 0.30–0.89 wt% throughout the section. RSEs normalized to Al or Ti exhibit concentrations equivalent to or less than world average shale (Fig. S2), and when RSEs are normalized to TOC there are no significant changes to enrichment profiles (Fig. S2). Ti/Al ratios are consistently below the average shale value with an average of 0.033 (Fig. S2). Organic carbon isotopes from the Rackla section show some variability but are generally invariant at ~−34‰ (Fig. S2).

4.3. Sheepbed Creek – sections J1456/S1405

Samples from the Hayhook and basal Sheepbed Formations are enriched in highly reactive iron with $Fe_{HR}/Fe_T > 0.38$ and $Fe_{Py}/Fe_{HR} < 0.7$ (Fig. 5), indicating deposition under a ferruginous water column. The highly reactive iron pool is dominated by iron oxide throughout the section. The abundance of iron oxides compared to Stoneknife Creek may indicate more sluggish early diagenetic processes at Sheepbed Creek, as iron carbonates and pyrite are the end products of iron reduction and sulfate reduction, respectively. From 77.2 to 105.8 m there is a shift to $Fe_{HR}/Fe_T < 0.38$, whereas samples between 105.8 and 179 m return to $Fe_{HR}/Fe_T > 0.38$. Above 179 m, Fe_{HR}/Fe_T values fluctuate below and above 0.38, potentially suggesting periods of transitory oxygenation. Vanadium, molybdenum, uranium, and chromium concentrations remain near world average shale concentrations until after ~75 m, where there is a rise in V and Mo concentrations to a maximum of 395 mg/kg and 8 mg/kg (respectively) before returning to concentrations similar to world average shale. Throughout the section, U and Cr concentrations remain relatively constant, with no noticeable variations in concentration despite interpreted differences in redox conditions from iron speciation and variations in V and Mo. Maximum values for U and Cr are 5.6 and 112 mg/kg respectively. TOC concentrations rise from 0.38 wt% in the basal samples to 1.86 wt% at ~100 m. TOC content then consistently decreases to 0.32 wt% at 294 m before spiking to 1.30 wt% in the uppermost part of the section. When RSEs are normalized to TOC, the inflection of enrichment at ~110 m becomes far less prominent (Fig. S3). Ti/Al is consistently below world average shale with an average of 0.034 (Fig. S3). Organic carbon isotopes at

this section start at approximately −31‰ and continuously decrease to −27‰ at the top of the section (Fig. S3).

5. Discussion

5.1. Age correlation between NW Canada and South China

Comparison of the geochemical data in NW Canada and evidence from OOE-A in South China is predicated on strata being correlative. A Re-Os date of 632.3 ± 5.9 Ma from the basal Sheepbed Fm. in NW Canada (Rooney et al., 2014) correlates well with the 632.5 ± 0.5 Ma ash bed dated near the base of Doushantuo II on the platform (Condon et al., 2005). However, while both formations were deposited directly above Marinoan-age glacial deposits, direct sample-to-sample correlation is unrealistic and poor temporal constraints in the overlying Ediacaran successions complicate anything beyond broad stratigraphic comparison.

In South China, correlations of Ediacaran strata between the intershelf and slope of the margin are predominantly based on lithological similarities and identification of a few key units and lithology (Jiang et al., 2011; Sahoo et al., 2012). Regional correlation is critical as strata in the Three Gorges area (intrashelf) provide the more robust temporal framework (Condon et al., 2005; Jiang et al., 2011), while the slope sections host the geochemical signatures of the OOEs (Wuhe, Taoying, Yuanjia; Sahoo et al., 2012; Sahoo et al., 2016). Sahoo et al. (2012, 2016) followed the correlations of Jiang et al. (2011), who suggest Doushantuo members I–IV can be differentiated on the slope sections, and that the entire Ediacaran is preserved in these successions. However, these variably condensed lower slope sections (<100 m–120 m) are poorly exposed or destroyed (the Wuhe section is now under water and Yuanjia was buried in a mudslide), are riddled with slumps and subtle slide surfaces (Vernhet et al., 2006), and lack distinctive lithological units for robust regional correlation. An alternative correlation based on carbon isotope chemostratigraphy at the Wuhe section supports correlation of almost the entire section with members III and IV on the platform. Certainly, the carbon isotope patterns do not match between Jiulongwan and Wuhe in a straightforward manner if both sections record the entirety of the Ediacaran (e.g., Fig. 6 of Jiang et al., 2007). Thus, while OOE-A is observed in strata directly above member I in the three basinal sections, the timing and duration of deposition remain completely unknown for each locality. Sahoo et al. (2012) assumed a similar rate of deposition between the intrashelf and slope deposits and that OOE-A was deposited prior to the deposition of an ash dated at 632.4 ± 0.5 Ma (Condon et al., 2005), but based on the observations above, litho- and chemo-stratigraphy do not necessarily support this correlation. Even with such conservative estimates for the ages of deposition, the evidence would suggest that the basal shale succession of member II in the Doushantuo is extremely condensed compared to normal marine shale.

In contrast to the condensed Doushantuo Formation sections, the Sheepbed sections on both the shelf and slope are greatly expanded, preserving a single transgressive-regressive sequence that spans over ~500 m (Macdonald et al., 2013). Organic carbon isotope patterns of the basal-most Sheepbed Fm. at Stoneknife Creek and Sheepbed Creek are consistent, beginning with invariant values of ~−31‰. Values at Rackla are ~2–3‰ lighter, perhaps due to aforementioned alteration at this section. The isotopic pattern at Sheepbed Creek throughout the Formation matches a similar trend recorded in the Wernecke Mountains and the Doushantuo Fm. of South China, of a progressive shift toward more positive values through the early Ediacaran and provides some chemostratigraphic constraints (Johnston et al., 2013; Jiang et al., 2010). This positive shift is consistent with the deposition of organic rich transgressive shale deposits in multiple basins worldwide during this period. Exact depositional rates are not known with certainty in either region, but based on average shale depositional rates and carbon isotopic correlations, we estimate that the ~500 m Sheepbed Fm. was deposited in 5–25 Myr. This suggests a staggering range of possible variation in sedimentation rate when compared to the Doushantuo—with rates in South China between 20 and 100 times slower than in NW Canada. In summary, while it is clear the stratigraphy broadly correlates between the two regions, exact correlation between NW Canada and basinal Doushantuo sections will ultimately be dependent on an improved geochronologic framework.

5.2. Possible biases affecting the early Ediacaran record in NW Canada

The shale geochemical record of earliest Ediacaran strata in NW Canada does not provide support for a transient OOE. Locally, iron speciation results suggest early Ediacaran samples were deposited under a persistently anoxic water column at Stoneknife Creek, Rackla, and Sheepbed Creek directly following the Marinoan glaciation (Figs. 3-5). These results are consistent with previously published iron speciation data from other localities in the region (Canfield et al., 2008; Johnston et al., 2013; Shen et al., 2008; Sperling et al., 2015). Geochemical evidence for localized ephemeral oxygenation does occur in some NW Canada localities during the Ediacaran (for instance at Sheepbed Creek in this study; see also Johnston et al., 2013; Sperling et al., 2016), but during the earliest Ediacaran the deeper waters facies appear to record anoxic conditions. In our data, the lack of 'Phanerozoic-style' RSE enrichments in strata along the NW Canadian margin imply limited marine RSE reservoirs, likely due to a large global expanse of anoxic conditions. Again, these results are consistent with other lower resolution datasets (Johnston et al., 2013; Kunzmann et al., 2015) that display muted RSE enrichments in shale deposited under ferruginous conditions during the earliest Ediacaran following the Marinoan Snowball Earth. Comparing early Ediacaran RSE concentrations from South China directly with that of NW Canada through standard boxplots, the two localities remain disparate in their levels of enrichment even after accounting for known factors that result in variability in the magnitude of enrichment (Fig. 6). Thus, there appears to be a discrepancy between multiple datasets from NW Canada and elsewhere with some published datasets from South China.

Considering this discrepancy, one possibility is that the iron speciation proxy has failed to correctly differentiate between oxic and ferruginous conditions in NW Canada. Interpretations of ferruginous conditions are based on enrichments in reactive iron species under anoxic conditions and consistency in the iron cycle throughout geologic time. Although not observed in the published calibration set from the modern ocean (Raiswell and Canfield, 1998), it may be possible to get Fe_{HR}/Fe_T ratios > 0.38 and a false anoxic signal due to either a proportionally large detrital reactive-iron flux or proportionally small flux of detrital unreactive iron. Local calibration to the detrital source would be required to test this possibility. Differences between modern sediment baseline values analyzed using dithionite-only extractions and the sequential extraction methodology used here could also play a role (see discussion in Farrell et al., 2013). There are also some known cases of iron enrichment under oxic conditions in modern environments. In the Peruvian OMZ, an iron-shuttle is thought to enrich oxic sediments below the OMZ in (presumably) highly reactive iron phases derived from poorly oxygenated shelf sediments (Scholz et al., 2014). However there is no evidence for an OMZ-type setting in the Ediacaran of NW Canada. Thus, while an erroneous signal in the iron speciation data (specifically a ferruginous signal resulting from an oxygenated water column) would help bring the NW Canada and South China geochemical records into parity, the most parsimonious interpretation is that the elevated Fe_{HR}/Fe_T in the Sheepbed Formation are a result of an anoxic water column during deposition.

Another possibility is that the NW Canada RSE enrichments are affected by the paleohydrogeography, regional sedimentation patterns or post-depositional alteration. Isolation of the water mass during deposition of the Sheepbed Formation could result in muted enrichments in RSEs (e.g., Algeo and Lyons, 2006; Algeo and Rowe, 2012). As noted in

Please cite this article as: Miller, A.J., et al., Tracking the onset of Phanerozoic-style redox-sensitive trace metal enrichments: New results from basal Ediacaran post-glacial str..., Chem. Geol. (2017), http://dx.doi.org/10.1016/j.chemgeo.2017.03.010

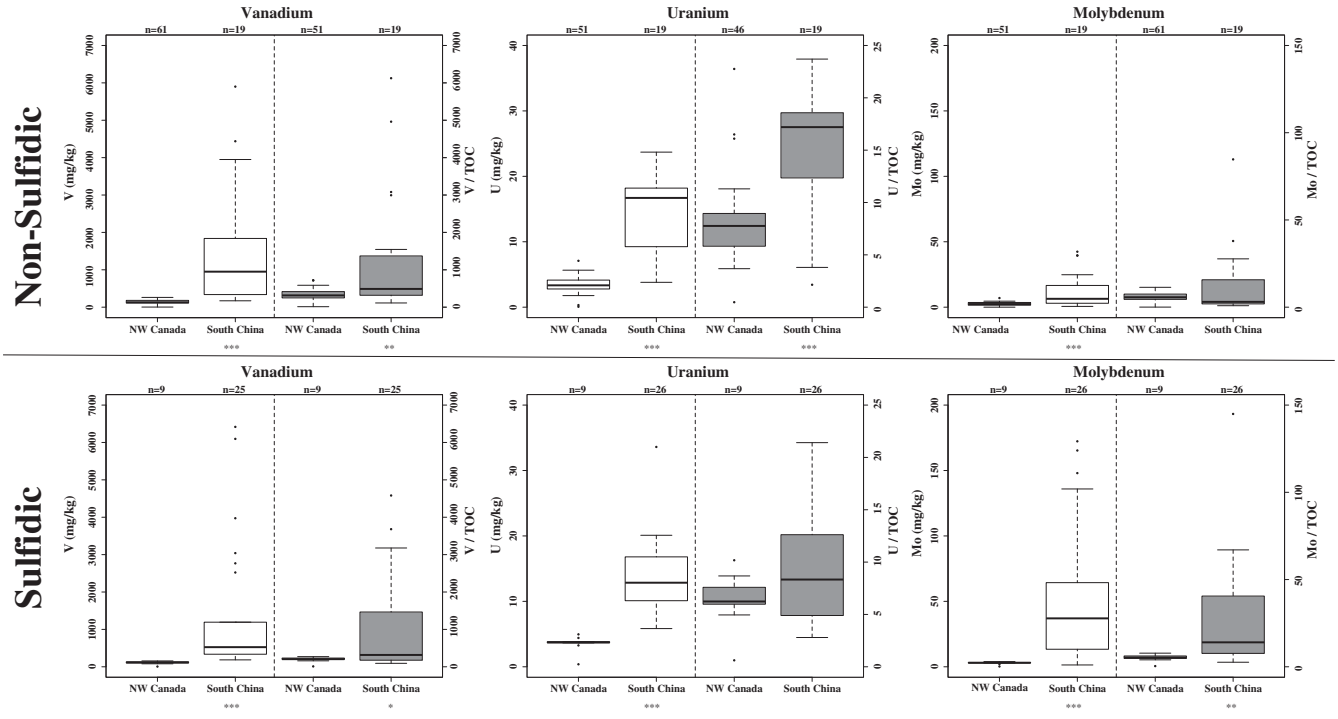

Fig. 6. Standard box plots comparing vanadium, uranium, and molybdenum as bulk concentrations and normalized to TOC between South China and NW Canada for the OOE-A interval. Shale samples are classified as sulfidic when $Fe_{Py}/Fe_{HR} > 0.7$ per designation of samples in Sahoo et al. (2012, 2016). Samples with TOC concentrations below 0.2 wt% were not included, as error on low TOC measurements can lead to spurious ratios. Additional data from the basal Sheepbed Fm. at Goz Creek reported by Johnston et al. (2013; up to 50 m in section F849) was also included in the NW Canada dataset. Mean RSE and RSE/TOC enrichments are significantly larger for South China (Mann-Whitney *U* test) for all comparisons except for non-sulfidic Mo/TOC ratios ($p = 0.59$) and sulfidic U/TOC ratios ($p = 0.27$). * = $p < 0.05$, ** = $p < 0.01$, *** = $p < 0.001$.

Section 2.3, the stratigraphic pattern of the "upper" Group suggests a substantially open margin, and unless future stratigraphic work alters this understanding, restriction is unlikely to be the primary driver of muted enrichments. RSE enrichments could be masked by rapid sedimentation resulting from turbidity currents and other mass-transport processes, which can limit the time of accumulation and therefore authigenic enrichment. However, these sedimentary controls on RSE enrichment also affect iron speciation (Poulton and Canfield, 2011), and the presence of enriched Fe_{HR}/Fe_T ratios in all investigated Sheepbed sections argues against this factor being relevant. Sheepbed Creek is the only locality where iron speciation results are interpreted as equivocal due to the presence of coarser beds in association with shale samples having $Fe_{HR}/Fe_T < 0.38$ (specifically between the interval of 77.2 m and 105.8 m, Fig. 5). The concordance of patterns in local redox signals throughout the Sheepbed Formation from sections across the basin further supports the conclusion that muted signals are not an artifact of localized sedimentation patterns (Canfield et al., 2008; Johnston et al., 2013; Sperling et al., 2015; this study).

Concentrations of RSEs can also be diluted by non-detrital sedimentary components, such as excessive calcium carbonate and silica precipitation. Petrographic analysis of a select group of samples did reveal the presence of authigenic carbonate, including rhombohedral dolomite, in many samples. RSEs were normalized to biogeochemically conservative elements (i.e., Al and Ti) to see through such effects and still showed no marked enrichment as compared to average shale (Figs. S1-S3). It is noteworthy that some of our samples have elevated Al concentrations above what is typically expected for shale (Turekian and Wedepohl, 1961). The Ti/Al ratios are thus consistently low compared to average shale through the earliest Ediacaran sections in NW Canada, which may suggest a predominantly felsic provenance, low aeolian input, a clay mineral dominated lithogenic component, and/or simply a spurious effect of Al enrichments from high production (Bertrand et al., 1996; Kryc et al., 2003; Murphy et al., 2000; Young and Nesbitt, 1998) (Figs. S1–S3). This is consistent with Nd isotope evidence that indicates a provenance dominated by old, evolved, continental crust at this time (Cox et al., 2016). However, there is no evidence of an especially unusual source terrane in NW Canada (Johnston et al., 2013).

The combination of low organic carbon input and/or preservation in the sediment is another potential driver of low RSE abundances. Geologically recent samples with high enrichments in RSEs are often associated with very elevated organic carbon content (Algeo and Lyons, 2006). However, samples from South China also exhibit relatively low TOC content in the basal Doushantuo (avg. 1.7 wt%, max. 4.1 wt% within OOE-A; Sahoo et al., 2012). The RSE/TOC ratios remain much lower for NW Canada compared to South China (Fig. 6; Figs. S1–S3 and Sahoo et al., 2012, 2016). Samples from the basal Sheepbed Formation in the euxinic interval at Stoneknife Creek have carbon/sulfur (C/S) ratios < 1, which is uncommon for euxinic deposition (Raiswell and Berner, 1985). Interestingly, many of the samples in the Doushantuo sections also have similar C/S ratios (Sahoo et al., 2012). At least in NW Canada, petrographic evidence suggests the elevated S values are not the result of epigenetic hydrothermal overprint (e.g., Leventhal, 1995). The reason for these relatively low C/S ratios in earliest Ediacaran sediments is presently unknown but may be related to differences in the type of organic carbon compared to the modern and later Phanerozoic (Raiswell and Berner, 1986) or to thermal maturation and loss of organic carbon (Raiswell and Berner, 1986, 1987). Neither case explains the trace metal discrepancies between the two regions.

All of the samples in this study were taken from outcrop (as with the Doushantuo Member II samples from South China; Sahoo et al., 2012), which could result in leaching of RSEs. However, active geomorphic processes in NW Canada provide relatively fresh outcrop with minimal vegetation, and the relatively cold climate of NW Canada stifles aggressive chemical weathering. Furthermore, Perkins and Mason (2015) found weathered black shale did not show a significant difference in the primary concentration of Mo, Cr or V when compared to core and fresh outcrop. The consistent and generally invariant trends of Mo, Cr, V and U concentrations in most sections in our study further suggest the

Please cite this article as: Miller, A.J., et al., Tracking the onset of Phanerozoic-style redox-sensitive trace metal enrichments: New results from basal Ediacaran post-glacial str..., Chem. Geol. (2017), http://dx.doi.org/10.1016/j.chemgeo.2017.03.010

muted nature of elemental enrichments is not an artifact of post-depositional weathering. In light of these considerations, and given that the lack of RSE enrichments in earliest Ediacaran strata from NW Canada matches similar data from Svalbard (Kunzmann et al., 2015), these data likely reflect primary Neoproterozoic marine geochemical processes. Below, we discuss two possibilities—muted enrichments under generally ferruginous conditions in NW Canada and over-enrichment in the Doushantuo Formation of South China—that may explain the regional discrepancies.

5.3. Redox-state effects on RSE enrichment

The lack of enrichments in RSEs observed in earliest Ediacaran strata in NW Canada and Svalbard may ultimately be a result of dominantly ferruginous local water columns at the time of deposition. Specifically, such environments may not provide a sufficiently reducing environment to sequester RSEs. Our understanding of RSE sequestration in ferruginous environments is limited by the fact that in the modern ocean there are no true ferruginous basins. Nonetheless, current knowledge of these RSEs and their behavior suggests that Mo is the only one that directly requires free sulfide in either the water column or shallow pore waters in order to become significantly enriched within the sediment (Little et al., 2015; Tribovillard et al., 2006; note that vanadium may be an exception due to the role of sulfide in a two-step reduction—see Section 2.2). Indeed, Cr, V, and U should all be enriched in sediment deposited under ferruginous ocean conditions if the marine reservoir is not depleted in these elements (Behrends and Van Cappellen, 2005; Breit and Wanty, 1991; Eary and Rai, 1989; Fendorf and Li, 1996; Massey et al., 2014; Partin et al., 2013a, b; Piper, 1994; Piper and Calvert, 2009; Rai et al., 1989; Reinhard et al., 2013; Stylo et al., 2015).

Consistent with this interpretive framework, significant enrichments in V and Cr are observed in the Doushantuo Fm. in samples that exhibit no geochemical signatures of deposition under a euxinic water column (Fig. 6; Sahoo et al., 2012, 2016). More importantly, the samples from Stoneknife Creek covering the Hayhook/Sheepbed transition (Fig. 3) have iron speciation ratios that arguably suggest a transient period of euxinia, but without pronounced enrichments in any RSE. Considering these facts, a redox-state hypothesis is not our preferred explanation for the regional discrepancy, but it is acknowledged that due to our current limited understanding of natural ferruginous depositional settings this hypothesis must remain valid.

5.4. The RSE record of the Doushantuo Formation

While it is possible that ferruginous depositional conditions may explain muted RSE enrichments in the basal Sheepbed Formation, an alternative possibility to explain the discrepancy is either primary or secondary processes resulting in over-enrichment in the Doushantuo Formation. Indeed, various geochemical aspects of the Doushantuo strata recording the OOEs are difficult to reconcile with straightforward authigenic enrichment from seawater carrying modern dissolved trace metal inventories. For instance, many of the samples in the Doushantuo have contrasting trace metal signals, with near-crustal concentrations of Mo and slightly elevated U in samples having extreme enrichments in V (OOE – A & B; Sahoo et al., 2012; Sahoo et al., 2016), or conversely enrichments of Mo typical of euxinic environments but low concentrations of both U and V (OOE – C; Sahoo et al., 2016). Large enrichments of these RSEs in sulfidic systems should broadly covary rather than behave independently. Complicated oceanographic patterns involving water masses sequentially moving through different redox environments could help to explain contrasting enrichment patterns (e.g., Fu et al., 2016 for the ore-grade early Cambrian Ni-Mo horizon in South China), but such processes are not the norm in most Phanerozoic or modern settings. Furthermore, there is little stratigraphic reproducibility of the OOE-A horizon across the South China paleo-margin. For example, other outcrops of the Doushantuo do not exhibit enrichments in RSEs directly above the cap carbonate in samples interpreted as deposited under euxinic conditions (Han and Fan, 2015; Li et al., 2010). While some of these discordant results have been attributed to localized basin isolation on the shelf (Och et al., 2015), others are harder to dismiss in the current interpretive frameworks (Han and Fan, 2015).

The OOE intervals in South China are also characterized by enrichments of RSEs (and RSEs in particular mineral phases) that are much larger than those observed in euxinic Phanerozoic shale. While OOE-interval bulk rock U and Mo concentrations are within the 'normal' range for Phanerozoic black shale, pyrite Mo concentrations are up to ~6000–8000 mg/kg (Sahoo, 2015), much higher than Phanerozoic shale where pyrite Mo levels are almost all <1000 mg/kg (Large et al., 2014). Bulk rock vanadium and rhenium (another RSE) are also extremely enriched in the Doushantuo Formation. In the Wuhe section, V is enriched up to 3.0 wt% (~30,000 mg/kg) within the purported OOEs (reported in supplement to Sahoo et al., 2016 but not plotted in their Fig. 2). Such enrichments in V have never been observed in sediments from modern reducing environments and are several times larger than "hyper-enriched" samples from the Phanerozoic that fall between 0.1 and 1 wt% (1000–10,000 mg/kg; Scott et al., 2013b; Scott et al., 2017). Rhenium concentrations range up to 3585 μg/kg in OOE-A, 1640 μg/kg in OOE-B and 1063 μg/kg in OOE-C (Sahoo, 2015; Sahoo et al., 2016). These Re concentrations are up to 10 times more enriched than those recorded in the most enriched Phanerozoic black shale samples (Harris et al., 2013; Selby, 2007; Xu et al., 2009) and up to 100 times more enriched than modern anoxic settings (Colodner et al., 1993). These magnitudes of enrichment likely require processes above and beyond a large seawater RSE reservoir. While it may be correct to exclude some of these extremely enriched samples (as in Sahoo et al., 2016), their intimate (bracketing) stratigraphic relationship with the samples providing the prima facie evidence of the OOEs raises questions about the source of enrichment for all of the examined strata.

One possible explanation for these enrichments is provenance. The basal Doushantuo Formation at Jiulongwan contains abundant saponite ($Ca_{0.25}(Mg,Fe)_3((Si,Al)_4O_{10})(OH)_2 \cdot n(H_2O)$) relative to other clay mineral assemblages (Bristow et al., 2009; Huang et al., 2013). Huang et al. (2013) recently interpreted this saponite to be the detrital weathering product of a mafic to ultramafic provenance. Because these mafic sources are presumably enriched in V and Cr relative to granitic sources (Rudnick and Gao, 2003; Turekian and Wedepohl, 1961), sedimentary provenance may have played an important role in these excessive enrichments (note though that Sahoo, 2015 suggested this was not the case for the detrital phase at the main investigated Wuhe section based on Ti/Al ratios). If the detrital component accounts for a large part of the signal, this would be most evident in the more proximal sections (i.e., Three Gorges area), but contrary to this prediction, V concentrations in these sections are depleted compared to world average shale in Doushantuo member II (Och et al., 2015). Regarding provenance influences on authigenic enrichments, there are modern areas, such as the island of Java in Indonesia, where rivers are sourced from primarily volcanic material. Here, riverine flux of V is between 230 and 280 nmol/l, an order of magnitude greater than the world average of 15 nmol/l (Shiller and Boyle, 1987), but there does not appear to be an effect on local seawater concentrations beyond the delta (Van der Sloot et al., 1989). It is unlikely then that a mafic source would provide sufficient dissolved V from a riverine flux to impart such high concentrations to basinal Doushantuo Formation strata if the margin was substantially open and able to mix effectively with ocean water. Consequently, while provenance may have played a secondary role or interacted with other factors, we do not regard it to be the fundamental driver of the enrichments observed in the Doushantuo Formation.

Among primary drivers, the greatly condensed nature of the Doushantuo Formation is the most likely player in these RSE enrichments. Sedimentary condensation in an anoxic environment would have allowed authigenic enrichment to occur over an extended period,

Please cite this article as: Miller, A.J., et al., Tracking the onset of Phanerozoic-style redox-sensitive trace metal enrichments: New results from basal Ediacaran post-glacial str..., Chem. Geol. (2017), http://dx.doi.org/10.1016/j.chemgeo.2017.03.010

resulting in greater abundances when compared to modern analogues that predominantly feature high sedimentation rates (Algeo and Lyons, 2006; Lehmann et al., 2016). In this scenario, stratigraphic variation in RSE enrichments would no longer track dynamic global ocean oxygenation, but rather localized sedimentation rates. Black shale intervals within the Doushantuo Formation are also often characterized by phosphatic nodules and hardgrounds, including fist-sized phosphate/pyrite concretions (Hohl, 2015; Jiang et al., 2011; Sahoo et al., 2016). The Doushantuo is not unique in exhibiting both phosphorite deposits and extreme enrichments in RSEs such as V and U. Indeed, some of the highest enrichments in RSEs in shale are found in the Permian Phosphoria Formation (Breit and Wanty, 1991) and the early Cambrian Niutitang Fm. (Lehmann et al., 2016). This relationship could be because francolite, a common mineral in phosphorite, possesses an open structure that permits numerous substitutions of trace elements and/or absorbance of these metals onto the crystal surface, resulting in higher enrichments of V, U and Mo (Jarvis et al., 1994). Recent work also suggests a potential link between sulfur-oxidizing bacteria and the formation of the Doushantuo's phosphorite deposits, which may have also had a secondary effect of developing enrichments in RSEs within these sediments (Bailey et al., 2013). More work on the relationship between RSEs and phosphorite is necessary to determine if these deposits are a driving factor in the abnormal enrichments observed in the Doushantuo.

Considering secondary processes, hydrothermal or basinal fluids have demonstrably altered some primary geochemical signals, especially in Member I, at multiple localities (Bristow et al., 2011; Derkowski et al., 2013; Hohl, 2015; Rodler et al., 2016). Shale is generally considered resistant to hydrothermal alteration due to its low permeability, but the juxtaposition of more permeable conglomerate and carbonate facies of the Nantuo Formation and Doushantuo Member I directly below the thin shale interval (Member II) hosting the RSE enrichments could result in localized post-depositional alteration and preferential fluid migration. This may also explain why the RSE enrichments tail off so dramatically in the first few meters of Doushantuo Member II. Both the trace metal and Fe-S relationships of Doushantuo Member II have been considered primary and not altered by hydrothermal processes based on the presence of framboidal pyrite (Sahoo et al., 2012), but similarly sized framboids can also be formed in low-grade metamorphic or hydrothermal settings (Scott et al., 2009), and framboids only make up a small proportion of the pyrite population at these sites (Wang et al., 2012).

We note that these possible primary and secondary processes have not been determined to affect the actual sections hosting the evidence for an OOE in the earliest Ediacaran. Rather than point to any specific process, in the preceding paragraphs we highlight the geochemical complexity of the Doushantuo Formation and suggest possibilities that may explain 1) the contrasting signals between trace metals, and 2) uber-enrichments well beyond those known from the Phanerozoic or modern settings. This complexity does not necessarily refute the OOE hypothesis, which is also supported by sulfur isotopic evidence in the Doushantuo and other localities (Kunzmann et al., 2017; Sahoo et al., 2012, 2016). The most straightforward test of the OOE hypothesis would be to find the same signal at other global localities. Given pervasive ferruginous conditions in the Neoproterozoic (Canfield et al., 2008; Guilbaud et al., 2015; Sperling et al., 2015), further study of additional localities will likely result in the same impasse reached here, specifically in determining whether the observed discrepancy is due to differences in sedimentation rates and water column conditions (ferruginous versus euxinic), or to the unique geochemistry of the Doushantuo Formation. An alternative approach to test the OOE hypothesis throughout the Ediacaran will be to develop a more robust age model for the Doushantuo Formation and perform detailed microstratigraphic studies of the geochemistry and early/late-stage diagenesis of the high-RSE intervals. Such studies will inform modeling attempts to explain samples with non-standard enrichment patterns (for instance several weight-percent V but near-crustal Mo) and are crucial for a better understanding of Ediacaran paleoenvironmental evolution. Furthermore, comparative studies of RSE enrichments in ferruginous Phanerozoic shale will help disentangle the various controls on enrichment and test whether the RSE levels seen in the Sheepbed Formation are an expected consequence of a Phanerozoic-level seawater trace metal inventory under locally ferruginous conditions.

6. Conclusion

Our geochemical analyses of the basal Sheepbed Formation (earliest Ediacaran) in NW Canada reveal an anoxic water column at two shelf localities and one slope setting. With the exception of a brief euxinic interval recorded at Stoneknife Creek, iron speciation analyses suggest the local water column was predominantly ferruginous, which is consistent with previous studies from this region (Canfield et al., 2008; Johnston et al., 2013; Shen et al., 2008). Redox-sensitive element concentrations at all studied localities are consistently low compared to shale deposited under anoxic conditions in the Phanerozoic: specifically, at, or below, average shale values. These data contrast sharply with evidence from the coeval but extremely condensed slope sections of the Doushantuo Formation at Wuhe, Taoying and Yuanjia, South China (Sahoo et al., 2012, 2016). There, the base of the Ediacaran sections—as well as several other horizons throughout the Wuhe section—record trace metal enrichments that reach, or in cases considerably exceed, trace metal enrichments in Phanerozoic black shale, and have been interpreted as recording widespread ocean oxygenation.

The NW Canada – South China comparison raises a quandary for unlocking the seafloor redox landscape at the sediment-water interface as represented by the shale RSE record. Shale from the Doushantuo Formation is ostensibly closer to well-studied Modern and Phanerozoic euxinic analogues, but based on extreme RSE abundances and incongruous enrichment patterns, is unlikely to be simply recording the seawater trace metal inventory. An alternative hypothesis proposed here is that the high-RSE intervals in the Doushantuo Formation reflect some combination of primary and/or secondary processes that have resulted in Phanerozoic-level (or greater) enrichments despite relatively low Ediacaran seawater trace metal reservoirs. On the other hand, muted enrichments in NW Canada may be due to limited trace metal uptake under ferruginous conditions. Sustained low RSE enrichments during the likely euxinic interval at Stoneknife Creek, as well as our current understanding of U, V and Cr behavior (all of which should be enriched under ferruginous conditions), do however argue against this possibility. Nonetheless, given our limited knowledge of trace metal cycling under ferruginous conditions, it remains possible the muted NW Canada enrichments may be an expected result of profoundly different sedimentation rates and redox-state.

Compared to the Doushantuo, the view from NW Canada is likely more representative of Neoproterozoic oceans worldwide (e.g., Kunzmann et al., 2015), but these results are more difficult to interpret through the lens of geochemists' normal euxinic analogues. In light of this, correct accounting for depositional redox state in future analyses of RSE dynamics through time may be particularly crucial. We suggest the basic sedimentological character of the earliest Ediacaran stratigraphic record may provide our best clue to marine dissolved oxygen concentrations during this interval of Earth's history. Following the Marinoan glaciation, black shale deposition was globally ubiquitous (Arnaud and Halverson, 2011). Where this black shale has been investigated geochemically, it shows evidence for deposition under an anoxic water column (Canfield et al., 2008; Guan et al., 2014; Johnston et al., 2013; Kunzmann et al., 2015; Shen et al., 2008; Sahoo et al., 2012, 2016; this study). The sheer abundance of earliest Ediacaran anoxic basins strongly contrasts with the modern ocean—where anoxia is exceedingly rare—and on intuitive grounds argues against a fully oxygenated ocean-atmosphere system at that time.

Please cite this article as: Miller, A.J., et al., Tracking the onset of Phanerozoic-style redox-sensitive trace metal enrichments: New results from basal Ediacaran post-glacial str..., Chem. Geol. (2017), http://dx.doi.org/10.1016/j.chemgeo.2017.03.010

Supplementary data to this article can be found online at http://dx.doi.org/10.1016/j.chemgeo.2017.03.010.

Acknowledgements

Funding was provided by a National Science Foundation grant (EAR 1324095 awarded to DTJ), the Rocky Mountain Association of Geologists Philip McKenna Scholarship (AJM), NASA Astrobiology Institute Foundations of Complex Life Team (DTJ, FAM), an NSERC Discover Grant (GPH), and an Agouron Institute Geobiology Postdoctoral Fellowship (JVS). We thank Erin Beirne, Marcus Kunzmann, Timothy Gibson, David Mucciarone, Douglas Turner and Peter Crockford for help in the laboratory, and Thomas Algeo, Maurice Colpron, Timothy Gibson, Kim Lau, David Moynihan, Paul Myrow, and Clint Scott for helpful discussions and reviews. We thank Hendrik Falck for considerable help in coordinating logistical support, and North American Tungsten Corporation for allowing access to their facilities and airstrip. We would also like to thank the Aurora Research Institute, license #2761 in 2014 for research permission at our field site at Sheepbed Creek and license #15480 for permission at Stoneknife Creek. We thank Trans North, Horizon and Summit helicopters for safe flying.

References

Aitken, J.D., 1991. Two late Proterozoic glaciations, Mackenzie Mountains, northwestern Canada. Geology 19 (5), 445–448.
Algeo, T.J., 2004. Can marine anoxic events draw down the trace element inventory of seawater? Geology 32 (12), 1057–1060.
Algeo, T.J., Lyons, T.W., 2006. Mo–total organic carbon covariation in modern anoxic marine environments: implications for analysis of paleoredox and paleohydrographic conditions. Paleoceanography 21 (1), PA1016.
Algeo, T.J., Maynard, J.B., 2004. Trace-element behavior and redox facies in core shales of Upper Pennsylvanian Kansas-type cyclothems. Chem. Geol. 206 (3), 289–318.
Algeo, T.J., Maynard, J.B., 2008. Trace-metal covariation as a guide to water-mass conditions in ancient anoxic marine environments. Geosphere 4 (5), 872–887.
Algeo, T.J., Rowe, H., 2012. Paleoceanographic applications of trace-metal concentration data. Chem. Geol. 324, 6–18.
Anderson, R.F., Fleisher, M.Q., LeHuray, A.P., 1989. Concentration, oxidation state, and particulate flux of uranium in the Black Sea. Geochim. Cosmochim. Acta 53 (9), 2215–2224.
Anderson, T.F., Raiswell, R., 2004. Sources and mechanisms for the enrichment of highly reactive iron in euxinic Black Sea sediments. Am. J. Sci. 304 (3), 203–233.
Arnaud, E., Halverson, G.P., Shields-Zhou, G. (Eds.), 2011. The Geological Record of Neoproterozoic Glaciations. Geological Society of London.
Bailey, J.V., Corsetti, F.A., Greene, S.E., Crosby, C.H., Liu, P., Orphan, V.J., 2013. Filamentous sulfur bacteria preserved in modern and ancient phosphatic sediments: implications for the role of oxygen and bacteria in phosphogenesis. Geobiology 11 (5), 397–405.
Bargar, J.R., Williams, K.H., Campbell, K.M., Long, P.E., Stubbs, J.E., Suvorova, E.I., Lezama-Pacheco, J.S., Alessi, D.S., Stylo, M., Webb, S.M., Davis, J.A., 2013. Uranium redox transition pathways in acetate-amended sediments. Proc. Natl. Acad. Sci. 110 (12), 4506–4511.
Behrends, T., Van Cappellen, P., 2005. Competition between enzymatic and abiotic reduction of uranium (VI) under iron reducing conditions. Chem. Geol. 220 (3), 315–327.
Bertrand, P., Shimmield, G., Martinez, P., Grousset, F., Jorissen, F., Paterne, M., Pujol, C., Bouloubassi, I., Menard, P.B., Peypouquet, J.P., Beaufort, L., 1996. The glacial ocean productivity hypothesis: the importance of regional temporal and spatial studies. Mar. Geol. 130 (1), 1–9.
Bertine, K.K., Turekian, K.K., 1973. Molybdenum in marine deposits. Geochim. Cosmochim. Acta 37 (6), 1415–1434.
Breit, G.N., Wanty, R.B., 1991. Vanadium accumulation in carbonaceous rocks: a review of geochemical controls during deposition and diagenesis. Chem. Geol. 91 (2), 83–97.
Bristow, T.F., Bonifacie, M., Derkowski, A., Eiler, J.M., Grotzinger, J.P., 2011. A hydrothermal origin for isotopically anomalous cap dolostone cements from south China. Nature 474 (7349), 68–71.
Bristow, T.F., Kennedy, M.J., Derkowski, A., Droser, M.L., Jiang, G., Creaser, R.A., 2009. Mineralogical constraints on the paleoenvironments of the Ediacaran Doushantuo Formation. Proc. Natl. Acad. Sci. 106 (32), 13190–13195.
Calvert, S., Pedersen, T., 1993. Geochemistry of recent oxic and anoxic marine sediments: Implications for the geological record. Mar. Geol. 113 (1), 67–88.
Canfield, D.E., Raiswell, R., Westrich, J.T., Reaves, C.M., Berner, R.A., 1986. The use of chromium reduction in the analysis of reduced inorganic sulfur in sediments and shales. Chem. Geol. 54 (1), 149–155.
Canfield, D.E., Poulton, S.W., Narbonne, G.M., 2007. Late-Neoproterozoic deep-ocean oxygenation and the rise of animal life. Science 315 (5808), 92–95.
Canfield, D.E., Poulton, S.W., Knoll, A.H., Narbonne, G.M., Ross, G., Goldberg, T., Strauss, H., 2008. Ferruginous conditions dominated later Neoproterozoic deep-water chemistry. Science 321 (5891) (949–942).
Chappaz, A., Lyons, T.W., Gregory, D.D., Reinhard, C.T., Gill, B.C., Li, C., Large, R.R., 2014. Does pyrite act as an important host for molybdenum in modern and ancient euxinic sediments? Geochim. Cosmochim. Acta 126, 112–122.
Colodner, D., Sachs, J., Ravizza, G., Turekian, K., Edmond, J., Boyle, E., 1993. The geochemical cycle of rhenium: a reconnaissance. Earth Planet. Sci. Lett. 117 (1–2), 205–221.
Colpron, M., Logan, J.M., Mortensen, J.K., 2002. U-Pb zircon age constraint for late Neoproterozoic rifting and initiation of the lower Paleozoic passive margin of western Laurentia. Can. J. Earth Sci. 39 (2), 133–143.
Condon, D., Zhu, M., Bowring, S., Wang, W., Yang, A., Jin, Y., 2005. U-Pb ages from the Neoproterozoic Doushantuo formation, China. Science 308 (5718), 95–98.
Cox, G.M., Halverson, G.P., Stevenson, R.K., Vokaty, M., Poirier, A., Kunzmann, M., Li, Z.X., Denyszyn, S.W., Strauss, J.V., Macdonald, F.A., 2016. Continental flood basalt weathering as a trigger for Neoproterozoic Snowball Earth. Earth Planet. Sci. Lett. 446, 89–99.
Dahl, T.W., Chappaz, A., Fitts, J.P., Lyons, T.W., 2013. Molybdenum reduction in a sulfidic lake: evidence from X-ray absorption fine-structure spectroscopy and implications for the Mo paleoproxy. Geochim. Cosmochim. Acta 103, 213–231.
Dalrymple, R., Narbonne, G., 1996. Continental slope sedimentation in the Sheepbed Formation (Neoproterozoic, Windermere Supergroup), Mackenzie Mountains, NWT. Can. J. Earth Sci. 33 (6), 848–862.
Derkowski, A., Bristow, T.F., Wampler, J.M., Środoń, J., Marynowski, L., Elliott, W.C., Chamberlain, C.P., 2013. Hydrothermal alteration of the Ediacaran Doushantuo Formation in the Yangtze Gorges area (south China). Geochim. Cosmochim. Acta 107, 279–298.
Eisbacher, G., 1981. Sedimentary tectonics and glacial record in the Windermere Supergroup, Mackenzie Mountains, northwestern Canada. Geol. Surv. Can. Pap. 80–27, 40.
Eisbacher, G., 1985. Late Proterozoic rifting, glacial sedimentation, and sedimentary cycles in the light of Windermere deposition, western Canada. Palaeogeogr. Palaeoclimatol. Palaeoecol. 51 (1), 231–254.
Emerson, S.R., Huested, S.S., 1991. Ocean anoxia and the concentrations of molybdenum and vanadium in seawater. Mar. Chem. 34 (3), 177–196.
Erickson, B.E., Helz, G.R., 2000. Molybdenum (VI) speciation in sulfidic waters: stability and lability of thiomolybdates. Geochim. Cosmochim. Acta 64 (7), 1149–1158.
Erwin, D.H., Laflamme, M., Tweedt, S.M., Sperling, E.A., Pisani, D., Peterson, K.J., 2011. The Cambrian conundrum: early divergence and later ecological success in the early history of animals. Science 334 (6059), 1091–1097.
Eary, L.E., Rai, D., 1989. Kinetics of chromate reduction by ferrous ions derived from hematite and biotite at 25 degrees C. Am. J. Sci. 289 (2), 180–213.
Elie, M., Nogueira, A.C., Nedelec, A., Trindade, R.I., Kenig, F., 2007. A red algal bloom in the aftermath of the Marinoan Snowball Earth. Terra Nova 19 (5), 303–308.
Farrell, Ú.C., Briggs, D.E., Hammarlund, E.U., Sperling, E.A., Gaines, R.R., 2013. Paleoredox and pyritization of soft-bodied fossils in the Ordovician Frankfort Shale of New York. Am. J. Sci. 313 (5), 452–489.
Fendorf, S.E., Li, G., 1996. Kinetics of chromate reduction by ferrous iron. Environ. Sci. Technol. 30 (5), 1614–1617.
Fike, D., Grotzinger, J., Pratt, L., Summons, R., 2006. Oxidation of the Ediacaran Ocean. Nature 444 (7120), 744–747.
Fu, Y., Dong, L., Li, C., Qu, W., Pei, H., Qiao, W., Shen, B., 2016. New Re-Os isotopic constrains on the formation of the metalliferous deposits of the Lower Cambrian Niutitang formation. J. Earth Sci. 27 (2), 271–281.
Gabrielse, H., Blusson, S.L., Roddick, J.H., 1973. Geology of Flat River, Glacier Lake and Wrigley Lake Map-areas, District of Mackenzie and Yukon Territory. Geol. Surv. Can. Mem. 366 (153), 52–55.
Gill, B.C., Lyons, T.W., Young, S.A., Kump, L.R., Knoll, A.H., Saltzman, M.R., 2011. Geochemical evidence for widespread euxinia in the Later Cambrian ocean. Nature 469 (7328), 80–83.
Guan, C., Zhou, C., Wang, W., Wan, B., Yuan, X., Chen, Z., 2014. Fluctuation of shelf basin redox conditions in the early Ediacaran: Evidence from Lantian Formation black shales in South China. Precambrian Res. 245, 1–12.
Guilbaud, R., Poulton, S.W., Butterfield, N.J., Zhu, M., Shields-Zhou, G.A., 2015. A global transition to ferruginous conditions in the early Neoproterozoic oceans. Nat. Geosci. 8 (6), 466–470.
Halverson, G.P., Wade, B.P., Hurtgen, M.T., Barovich, K.M., 2010. Neoproterozoic chemostratigraphy. Precambrian Res. 182 (4), 337–350.
Han, T., Fan, H., 2015. Dynamic evolution of the Ediacaran ocean across the Doushantuo Formation, South China. Chem. Geol. 417, 261–272.
Harris, N.B., Mnich, C.A., Selby, D., Korn, D., 2013. Minor and trace element and Re–Os chemistry of the Upper Devonian Woodford Shale, Permian Basin, west Texas: insights into metal abundance and basin processes. Chem. Geol. 356, 76–93.
Helz, G., Miller, C., Charnock, J., Mosselmans, J., Pattrick, R., Garner, C., Vaughan, D., 1996. Mechanism of molybdenum removal from the sea and its concentration in black shales: EXAFS evidence. Geochim. Cosmochim. Acta 60 (19), 3631–3642.
Hickson, C.J., Juras, S.J., 1986. Sample contamination by grinding. Can. Mineral. 24 (3), 585–589.
Hohl, S.V., 2015. Multi-proxy Study of Ediacaran Shallow and Deep Water Carbonates - Yangtze Platform, South China. (Doctoral dissertation). Freie Universität Berlin.
Hsi, C.K.D., Langmuir, D., 1985. Adsorption of uranyl onto ferric oxyhydroxides: application of the surface complexation site-binding model. Geochim. Cosmochim. Acta 49 (9), 1931–1941.
Huang, J., Chu, X., Lyons, T.W., Planavsky, N.J., Wen, H., 2013. A new look at saponite formation and its implications for early animal records in the Ediacaran of South China. Geobiology 11 (1), 3–14.
Huang, J., Huang, F., Evans, L., Glasauer, S., 2015. Vanadium: Global (bio) geochemistry. Chem. Geol. 417, 68–89.

Please cite this article as: Miller, A.J., et al., Tracking the onset of Phanerozoic-style redox-sensitive trace metal enrichments: New results from basal Ediacaran post-glacial str..., Chem. Geol. (2017), http://dx.doi.org/10.1016/j.chemgeo.2017.03.010

James, N.P., Narbonne, G.M., Kyser, T.K., 2001. Late Neoproterozoic cap carbonates: Mackenzie Mountains, northwestern Canada: precipitation and global glacial meltdown. Can. J. Earth Sci. 38 (8), 1229–1262.
Jarvis, I., Burnett, W., Nathan, Y., Almbaydin, F., Attia, A., Castrol, L., Flicoteaux, R., Hilmy, M.E., Husain, V., Qutawnah, A., 1994. Phosphorite geochemistry: state of the art and environmental concerns. Eclogae Geol. Helv. 87 (3), 643–700.
Jefferson, C., Parrish, R., 1989. Late Proterozoic stratigraphy, U-Pb zircon ages, and rift tectonics, Mackenzie Mountains, northwestern Canada. Can. J. Earth Sci. 26 (9), 1784–1801.
Jiang, G., Kaufman, A.J., Christie-Blick, N., Zhang, S., Wu, H., 2007. Carbon isotope variability across the Ediacaran Yangtze platform in South China: implications for a large surface-to-deep ocean $\delta^{13}C$ gradient. Earth Planet. Sci. Lett. 261 (1), 303–320.
Jiang, G., Wang, X., Shi, X., Zhang, S., Xiao, S., Dong, J., 2010. Organic carbon isotope constraints on the dissolved organic carbon (DOC) reservoir at the Cryogenian-Ediacaran transition. Earth Planet. Sci. Lett. 299, 159–168.
Jiang, G., Shi, X., Zhang, S., Wang, Y., Xiao, S., 2011. Stratigraphy and paleogeography of the Ediacaran Doushantuo Formation (ca. 635–551 Ma) in South China. Gondwana Res. 19 (4), 831–849.
Johnston, D.T., Poulton, S.W., Tosca, N.J., O'Brien, T., Halverson, G.P., Schrag, D.P., Macdonald, F.A., 2013. Searching for an oxygenation event in the fossiliferous Ediacaran of northwestern Canada. Chem. Geol. 362 (0), 273–286.
Kirschvink, J.L., Gaidos, E.J., Bertani, L.E., Beukes, N.J., Gutzmer, J., Maepa, L.N., Steinberger, R.E., 2000. Paleoproterozoic snowball earth: extreme climatic and geochemical global change and its biological consequences. Proc. Natl. Acad. Sci. U. S. A. 97 (4), 1400–1405.
Klinkhammer, G., Palmer, M., 1991. Uranium in the oceans: where it goes and why. Geochim. Cosmochim. Acta 55 (7), 1799–1806.
Knoll, A., Walter, M., Narbonne, G., Christie-Blick, N., 2006. The Ediacaran Period: a new addition to the geologic time scale. Lethaia 39 (1), 13–30.
Kryc, K.A., Murray, R.W., Murray, D.W., 2003. Al-to-oxide and Ti-to-organic linkages in biogenic sediment: relationships to paleo-export production and bulk Al/Ti. Earth Planet. Sci. Lett. 211 (1), 125–141.
Ku, T., Knauss, K.G., Mathieu, G.G., 1977. Uranium in open ocean: concentration and isotopic composition. Deep-Sea Res. 24 (11), 1005–1017.
Kunzmann, M., Halverson, G.P., Sossi, P.A., Raub, T.D., Payne, J.L., Kirby, J., 2013. Zn isotope evidence for immediate resumption of primary productivity after snowball Earth. Geology 41 (1), 27–30.
Kunzmann, M., Halverson, G.P., Scott, C., Minarik, W.G., Wing, B.A., 2015. Geochemistry of Neoproterozoic black shales from Svalbard: implications for oceanic redox conditions spanning Cryogenian glaciations. Chem. Geol. 417, 383–393.
Kunzmann, M., Bui, T.H., Crockford, P.W., Halverson, G.P., Scott, C., Lyons, T.W., Wing, B.A., 2017. Bacterial sulfur disproportionation constrains timing of Neoproterozoic oxygenation. Geology (in press).
Large, R.R., Halpin, J.A., Danyushevsky, L.V., Maslennikov, V.V., Bull, S.W., Long, J.A., Gregory, D.D., Lounejeva, E., Lyons, T.W., Sack, P.J., McGoldrick, P.J., 2014. Trace element content of sedimentary pyrite as a new proxy for deep-time ocean–atmosphere evolution. Earth Planet. Sci. Lett. 389, 209–220.
Lehmann, B., Frei, R., Xu, L., Mao, J., 2016. Early Cambrian black shale-hosted Mo-Ni and V mineralization on the rifted margin of the Yangtze Platform, China: reconnaissance chromium isotope data and a refined metallogenic model. Econ. Geol. 111, 89–103.
Leventhal, J.S., 1995. Carbon-sulfur plots to show diagenetic and epigenetic sulfidation in sediments. Geochim. Cosmochim. Acta 59 (6), 1207–1211.
Li, C., Love, G.D., Lyons, T.W., Fike, D.A., Sessions, A.L., Chu, X., 2010. A stratified redox model for the Ediacaran ocean. Science 328 (5974), 80–83.
Little, S.H., Vance, D., Lyons, T.W., McManus, J., 2015. Controls on trace metal authigenic enrichment in reducing sediments: Insights from modern oxygen-deficient settings. Am. J. Sci. 315 (2), 77–119.
Lovley, D.R., Phillips, E.J., 1992. Reduction of uranium by *Desulfovibrio desulfuricans*. Appl. Environ. Microbiol. 58 (3), 850–856.
Lund, K., Aleinikoff, J.N., Evans, K.V., Fanning, C.M., 2003. SHRIMP U-Pb geochronology of Neoproterozoic Windermere Supergroup, central Idaho: Implications for rifting of western Laurentia and synchroneity of Sturtian glacial deposits. Geol. Soc. Am. Bull. 115 (3), 349–372.
Lund, K., Aleinikoff, J.N., Evans, K.V., Dewitt, E.H., Unruh, D.M., 2010. SHRIMP U-Pb dating of recurrent Cryogenian and Late Cambrian–early Ordovician alkalic magmatism in central Idaho: implications for Rodinian rift tectonics. Geol. Soc. Am. Bull. 122 (3–4), 430–453.
Lyons, T.W., Reinhard, C.T., Planavsky, N.J., 2014. The rise of oxygen in Earth's early ocean and atmosphere. Nature 506 (7488), 307–315.
Macdonald, F.A., Schmitz, M.D., Crowley, J.L., Roots, C.F., Jones, D.S., Maloof, A.C., Strauss, J.V., Cohen, P.A., Johnston, D.T., Schrag, D.P., 2010. Calibrating the Cryogenian. Science 327 (5970), 1241–1243.
Macdonald, F.A., Strauss, J.V., Sperling, E.A., Halverson, G.P., Narbonne, G.M., Johnston, D.T., Kunzmann, M., Schrag, D.P., Higgins, J.A., 2013. The stratigraphic relationship between the Shuram carbon isotope excursion, the oxygenation of Neoproterozoic oceans, and the first appearance of the Ediacara biota and bilaterian trace fossils in northwestern Canada. Chem. Geol. 362, 250–272.
MacNaughton, R.B., Narbonne, G.M., Dalrymple, R.W., 2000. Neoproterozoic slope deposits, Mackenzie Mountains, northwestern Canada: implications for passive-margin development and Ediacaran faunal ecology. Can. J. Earth Sci. 37 (7), 997–1020.
MacNaughton, R.B., Roots, C.F., Martel, E., 2008. Neoproterozoic-Cambrian Lithostratigraphy, northeast Sekwi Mountain map area, Mackenzie Mountains, Northwest Territories: new data from measured sections. Geol. Surv. of Can. Cur. Res. 16, 17.
März, C., Poulton, S., Beckmann, B., Küster, K., Wagner, T., Kasten, S., 2008. Redox sensitivity of P cycling during marine black shale formation: dynamics of sulfidic and anoxic, non-sulfidic bottom waters. Geochim. Cosmochim. Acta 72 (15), 3703–3717.
Massey, M.S., Lezama-Pacheco, J.S., Jones, M.E., Ilton, E.S., Cerrato, J.M., Bargar, J.R., Fendorf, S., 2014. Competing retention pathways of uranium upon reaction with Fe (II). Geochim. Cosmochim. Acta 142, 166–185.
McLennan, S.M., 2001. Relationships between the trace element composition of sedimentary rocks and upper continental crust. Geochem. Geophys. Geosyst. 2 (4) (2000GC000109).
McManus, J., Berelson, W.M., Klinkhammer, G.P., Hammond, D.E., Holm, C., 2005. Authigenic uranium: relationship to oxygen penetration depth and organic carbon rain. Geochim. Cosmochim. Acta 69 (1), 95–108.
Morford, J.L., Emerson, S., 1999. The geochemistry of redox-sensitive trace metals in sediments. Geochim. Cosmochim. Acta 63 (11), 1735–1750.
Morford, J.L., Emerson, S.R., Breckel, E.J., Kim, S.H., 2005. Diagenesis of oxyanions (V, U, Re, and Mo) in pore waters and sediments from a continental margin. Geochim. Cosmochim. Acta 69 (21), 5021–5032.
Murphy, A.E., Sageman, B.B., Hollander, D.J., Lyons, T.W., Brett, C.E., 2000. Black shale deposition and faunal overturn in the Devonian Appalachian basin: clastic starvation, seasonal water-column mixing, and efficient biolimiting nutrient recycling. Paleoceanography 15 (3), 280–291.
Narbonne, G.M., Aitken, J.D., 1990. Ediacaran fossils from the Sekwi Brook area, Mackenzie mountains, northwestern Canada. Palaeontology 33 (4), 945–980.
Narbonne, G.M., Aitken, J.D., 1995. Neoproterozoic of the Mackenzie Mountains, northwestern Canada. Precambrian Res. 73 (1), 101–121.
Narbonne, G.M., Laflamme, M., Trusler, P.W., Dalrymple, R.W., Greentree, C., 2014. Deep-water Ediacaran fossils from northwestern Canada: taphonomy, ecology, and evolution. J. Paleontol. 88 (02), 207–223.
Och, L.M., Cremonese, L., Shields-Zhou, G.A., Poulton, S.W., Struck, U., Ling, H., Li, D., Chen, X., Manning, C., Thirlwall, M., Strauss, H., 2015. Palaeoceanographic controls on spatial redox distribution over the Yangtze Platform during the Ediacaran–Cambrian transition. Sedimentology 63, 378–410.
Owens, J.D., Reinhard, C.T., Rohrssen, M., Love, G.D., Lyons, T.W., 2016. Empirical links between trace metal cycling and marine microbial ecology during a large perturbation to Earth's carbon cycle. Earth Planet. Sci. Lett. 449, 407–417.
Partin, C., Lalonde, S.V., Planavsky, N., Bekker, A., Rouxel, O., Lyons, T., Konhauser, K., 2013a. Uranium in iron formations and the rise of atmospheric oxygen. Chem. Geol. 362, 82–90.
Partin, C., Bekker, A., Planavsky, N., Scott, C., Gill, B., Li, C., Podkovyrov, V., Maslov, A., Konhauser, K., Lalonde, S., 2013b. Large-scale fluctuations in Precambrian atmospheric and oceanic oxygen levels from the record of U in shales. Earth Planet. Sci. Lett. 369, 284–293.
Pearce, C.R., Cohen, A.S., Coe, A.L., Burton, K.W., 2008. Molybdenum isotope evidence for global ocean anoxia coupled with perturbations to the carbon cycle during the early Jurassic. Geology 36 (3), 231–234.
Perkins, R.B., Mason, C.E., 2015. The relative mobility of trace elements from short-term weathering of a black shale. Appl. Geochem. 56, 67–79.
Piper, D.Z., 1994. Seawater as the source of minor elements in black shales, phosphorites and other sedimentary rocks. Chem. Geol. 114 (1), 95–114.
Piper, D., Calvert, S., 2009. A marine biogeochemical perspective on black shale deposition. Earth Sci. Rev. 95 (1), 63–96.
Piper, D.Z., Isaacs, C.M., 1996. Instability of bottom-water redox conditions during accumulation of quaternary sediment in the Japan Sea. Paleoceanography 11 (2), 171–190.
Planavsky, N.J., Rouxel, O.J., Bekker, A., Lalonde, S.V., Konhauser, K.O., Reinhard, C.T., Lyons, T.W., 2010. The evolution of the marine phosphate reservoir. Nature 467 (7319), 1088–1090.
Poulton, S.W., Canfield, D.E., 2011. Ferruginous conditions: a dominant feature of the ocean through Earth's history. Elements 7 (2), 107–112.
Poulton, S.W., Canfield, D.E., 2005. Development of a sequential extraction procedure for iron: Implications for iron partitioning in continentally derived particulates. Chem. Geol. 214 (3–4), 209–221.
Rai, D., Eary, L., Zachara, J., 1989. Environmental chemistry of chromium. Sci. Total Environ. 86 (1–2), 15–23.
Raiswell, R., Berner, R.A., 1985. Pyrite formation in euxinic and semi-euxinic sediments. Am. J. Sci. 285 (8), 710–724.
Raiswell, R., Berner, R.A., 1986. Pyrite and organic matter in Phanerozoic normal marine shales. Geochim. Cosmochim. Acta 50 (9), 1967–1976.
Raiswell, R., Berner, R.A., 1987. Organic carbon losses during burial and thermal maturation of normal marine shales. Geology 15 (9), 853–856.
Raiswell, R., Canfield, D.E., 1998. Sources of iron for pyrite formation in marine sediments. Am. J. Sci. 298 (3), 219–245.
Reinhard, C.T., Planavsky, N.J., Robbins, L.J., Partin, C.A., Gill, B.C., Lalonde, S.V., Bekker, A., Konhauser, K.O., Lyons, T.W., 2013. Proterozoic ocean redox and biogeochemical stasis. Proc. Natl. Acad. Sci. U. S. A. 110 (14), 5357–5362.
Rice, C.A., Tuttle, M.L., Reynolds, R.L., 1993. The analysis of forms of sulfur in ancient sediments and sedimentary rocks: comments and cautions. Chem. Geol. 107 (1), 83–95.
Rodler, A., Hohl, S., Guo, Q., Frei, R., 2016. Chromium isotope stratigraphy of Ediacaran cap dolostones, Doushantuo Formation, South China. Chem. Geol. 436, 24–34.
Rooney, A.D., Strauss, J.V., Brandon, A.D., Macdonald, F.A., 2015. A Cryogenian chronology: two long-lasting synchronous Neoproterozoic glaciations. Geology 43 (5), 459–462.
Rooney, A.D., Macdonald, F.A., Strauss, J.V., Dudas, F.O., Hallmann, C., Selby, D., 2014. Re-Os geochronology and coupled Os-Sr isotope constraints on the Sturtian Snowball Earth. Proc. Natl. Acad. Sci. U. S. A. 111, 51–56.
Ross, G., 1991. Tectonic setting of the Windermere Supergroup revisited. Geology 19 (11), 1125–1128.
Rudnick, R.L., Gao, S., 2003. Composition of the continental crust. In: Holland, H.D., Turekian, K.K. (Eds.), Treatise on Geochemistry. 3. Elsevier-Pergamon, Oxford, pp. 1–60.

Please cite this article as: Miller, A.J., et al., Tracking the onset of Phanerozoic-style redox-sensitive trace metal enrichments: New results from basal Ediacaran post-glacial str..., Chem. Geol. (2017), http://dx.doi.org/10.1016/j.chemgeo.2017.03.010

Sahoo, S.K., 2015. Ediacaran ocean redox evolution. UNLV Theses, Dissertations, Professional Papers, and Capstones (Paper 2577).
Sahoo, S., Planavsky, N., Jiang, G., Kendall, B., Owens, J., Wang, X., Shi, X., Anbar, A., Lyons, T., 2016. Oceanic oxygenation events in the anoxic Ediacaran ocean. Geobiology 14 (5), 457–468.
Sahoo, S.K., Planavsky, N.J., Kendall, B., Wang, X., Shi, X., Scott, C., Anbar, A.D., Lyons, T.W., Jiang, G., 2012. Ocean oxygenation in the wake of the Marinoan glaciation. Nature 489 (7417), 546–549.
Scholz, F., Severmann, S., McManus, J., Hensen, C., 2014. Beyond the Black Sea paradigm: the sedimentary fingerprint of an open-marine iron shuttle. Geochim. Cosmochim. Acta 127, 368–380.
Scott, C., Lyons, T., Bekker, A., Shen, Y., Poulton, S., Chu, X., Anbar, A., 2008. Tracing the stepwise oxygenation of the Proterozoic ocean. Nature 452 (7186), 456–459.
Scott, C., Slack, J.F., Kelley, K.D., 2017. The hyper-enrichment of V and Zn in black shales of the Late Devonian-Early Mississippian Bakken Formation (USA). Chem. Geol. (in press, corrected proof).
Scott, C., Lyons, T.W., 2012. Contrasting molybdenum cycling and isotopic properties in euxinic versus non-euxinic sediments and sedimentary rocks: refining the paleoproxies. Chem. Geol. 324, 19–27.
Scott, C., Planavsky, N.J., Dupont, C.L., Kendall, B., Gill, B.C., Robbins, L.J., Husband, K.F., Arnold, G.L., Wing, B.A., Poulton, S.W., 2013a. Bioavailability of zinc in marine systems through time. Nat. Geosci. 6 (2), 125–128.
Scott, C., Slack, J.F., Kelley, K.D., 2013b. The origin of Vanadium hyper-enriched black shales. Geol. Soc. Am. Abstr. Programs 45, 427.
Scott, R.J., Meffre, S., Woodhead, J., Gilbert, S.E., Berry, R.F., Emsbo, P., 2009. Development of framboidal pyrite during diagenesis, low-grade regional metamorphism, and hydrothermal alteration. Econ. Geol. 104 (8), 1143–1168.
Selby, D., 2007. Direct Rhenium-Osmium age of the Oxfordian-Kimmeridgian boundary, Staffin bay, Isle of Skye, UK, and the Late Jurassic time scale. Nor. Geol. Tidsskr. 87 (3), 291.
Shen, Y., Zhang, T., Hoffman, P.F., 2008. On the coevolution of Ediacaran oceans and animals. Proc. Natl. Acad. Sci. U. S. A. 105 (21), 7376–7381.
Shiller, A.M., Boyle, E.A., 1987. Dissolved vanadium in rivers and estuaries. Earth Planet. Sci. Lett. 86 (2–4), 214–224.
Sperling, E.A., Frieder, C.A., Raman, A.V., Girguis, P.R., Levin, L.A., Knoll, A.H., 2013a. Oxygen, ecology, and the Cambrian radiation of animals. Proc. Natl. Acad. Sci. U. S. A. 110 (33), 13446–13451.
Sperling, E.A., Halverson, G.P., Knoll, A.H., Macdonald, F.A., Johnston, D.T., 2013b. A basin redox transect at the dawn of animal life. Earth Planet. Sci. Lett. 371, 143–155.
Sperling, E.A., Wolock, C.J., Morgan, A.S., Gill, B.C., Kunzmann, M., Halverson, G.P., Macdonald, F.A., Knoll, A.H., Johnston, D.T., 2015. Statistical analysis of iron geochemical data suggests limited late Proterozoic oxygenation. Nature 523 (7561), 451–454.
Sperling, E.A., Carbone, C., Strauss, J.V., Johnston, D.T., Narbonne, G.M., Macdonald, F.A., 2016. Oxygen, facies, and secular controls on the appearance of Cryogenian and Ediacaran body and trace fossils in the Mackenzie Mountains of northwestern Canada. Geol. Soc. Am. Bull. 128 (3–4), 558–575.
Stookey, L.L., 1970. Ferrozine—a new spectrophotometric reagent for iron. Anal. Chem. 42 (7), 779–781.
Strauss, J.V., MacDonald, F.A., Halverson, G.P., Tosca, N.J., Schrag, D.P., Knoll, A.H., 2015. Stratigraphic evolution of the Neoproterozoic Callison Lake Formation: linking the break-up of Rodinia to the Islay carbon isotope excursion. Am. J. Sci. 315 (10), 881–944.
Stylo, M., Neubert, N., Wang, Y., Monga, N., Romaniello, S.J., Weyer, S., Bernier-Latmani, R., 2015. Uranium isotopes fingerprint biotic reduction. Proc. Natl. Acad. Sci. 112 (18), 5619–5624.
Tribovillard, N., Algeo, T.J., Lyons, T., Riboulleau, A., 2006. Trace metals as paleoredox and paleoproductivity proxies: an update. Chem. Geol. 232 (1), 12–32.
Turekian, K.K., Wedepohl, K.H., 1961. Distribution of the elements in some major units of the earth's crust. Geol. Soc. Am. Bull. 72 (2), 175–192.
Turner, E., Roots, C., MacNaughton, R., Long, D., Fischer, B., Gordey, S., Martel, E., Pope, M., 2011. Chapter 3. Stratigraphy. Geology of the Central Mackenzie Mountains of the Northern Canadian Cordillera, Sekwi Mountain (105P), Mount Eduni (106A), and Northwestern Wrigley Lake (95M) Map-Areas, Northwest Territories. NWT Geoscience Office, Yellowknife. pp. 31–192.
Van der Sloot, H.A., Hoede, D., Wijkstra, J., 1989. Trace oxyanions and their behaviour in the rivers Porong and Solo, the Java Sea and the adjacent Indian Ocean. Neth. J. Sea Res. 23 (4), 379–386.
der Weijden, Van, Cornelis, H., Middelburg, J.J., De Lange, G.J., der Sloot, Van, Hans, A., Hoede, D., Woittiez, J.R., 1990. Profiles of the redox-sensitive trace elements As, Sb, V, Mo and U in the Tyro and Bannock Basins (eastern Mediterranean). Mar. Chem. 31 (1–3), 171–186.
Vernhet, E., Heubeck, C., Zhu, M.Y., Zhang, J.M., 2006. Large-scale slope instability at the southern margin of the Ediacaran Yangtze platform (Hunan province, central China). Precambrian Res. 148 (1), 32–44.
Wang, L., Shi, X., Jiang, G., 2012. Pyrite morphology and redox fluctuations recorded in the Ediacaran Doushantuo Formation. Palaeogeogr. Palaeoclimatol. Palaeoecol. 333, 218–227.
Wanty, R.B., Goldhaber, M.B., 1992. Thermodynamics and kinetics of reactions involving vanadium in natural systems: accumulation of vanadium in sedimentary rocks. Geochim. Cosmochim. Acta 56 (4), 1471–1483.
Yonkee, W., Dehler, C., Link, P., Balgord, E., Keeley, J., Hayes, D., Wells, M., Fanning, C., Johnston, S., 2014. Tectono-stratigraphic framework of Neoproterozoic to Cambrian strata, west-central US: protracted rifting, glaciation, and evolution of the North American Cordilleran margin. Earth Sci. Rev. 136, 59–95.
Young, G., Jefferson, C., Delaney, G., Yeo, G., 1979. Middle and late Proterozoic evolution of the northern Canadian Cordillera and Shield. Geology 7 (3), 125–128.
Young, G.M., Nesbitt, H.W., 1998. Processes controlling the distribution of Ti and Al in weathering profiles, siliciclastic sediments and sedimentary rocks. J. Sediment. Res. 68 (3).
Xiao, S., Laflamme, M., 2009. On the eve of animal radiation: phylogeny, ecology and evolution of the Ediacara biota. Trends Ecol. Evol. 24 (1), 31–40.
Xu, G., Hannah, J.L., Stein, H.J., Bingen, B., Yang, G., Zimmerman, A., Weitschat, W., Mørk, A., Weiss, H.M., 2009. Re–Os geochronology of Arctic black shales to evaluate the Anisian–Ladinian boundary and global faunal correlations. Earth Planet. Sci. Lett. 288 (3), 581–587.
Zheng, Y., Anderson, R.F., van Geen, A., Fleisher, M.Q., 2002. Remobilization of authigenic uranium in marine sediments by bioturbation. Geochim. Cosmochim. Acta 66 (10), 1759–1772.

Please cite this article as: Miller, A.J., et al., Tracking the onset of Phanerozoic-style redox-sensitive trace metal enrichments: New results from basal Ediacaran post-glacial str..., Chem. Geol. (2017), http://dx.doi.org/10.1016/j.chemgeo.2017.03.010